Internship Report – University California Davis

April 23

2014

Offshore wind turbines are increasing in size through the years to reduce maintenance and increase efficiency. The increasing size of wind turbines have led to an increase in loads. There are several ways to deal with this but in this research active load control is studied. Microjets were already studied by A.M. Cooperman: Wind Tunnel Testing of Microtabs and Microjets for Active Load Control of Wind Turbine Blades and M.L. Blaylock: Computational Investigation on the Application of Using Microjets as Active Aerodynamic Load Control for Wind Turbines both studies done at the Mechanical and Aerospace Engineering. This research was initially an extension on the research of A.M. Cooperman eventually to check the findings of M.L. Blaylock. The microjet system uses small pneumatic jets to change the lift coefficient of the airfoil to quickly counter act loads induced by wind gusts. At the Mechanical and Aerospace wind tunnel research facility at UC Davis a series of static tests were done with a modified S819 airfoil in an open circuit wind tunnel at a Reynolds number of 500,000 for microjet flows with a momentum coefficient up to 0.005, the change in lift coefficient is studied as a function of the angle of attack alpha. With this information the open and, in a later stadium closed loop control can be formulated. In this study it was found that there is a linear correlation between the measured momentum coefficient and the angle of attack alpha, when the supply pressure is kept constant.

Active load control for wind turbine blades using micro-jets

Preface

In November 2012 I was hinted on an internship position at the Mechanical and Aerospace Engineering department of University California Davis by H.W.M. Hoeijmakers professor and chair president for the Engineering Fluid Dynamics department at University Twente. The research I did at UC Davis on active load control using micro jets was supervised by Professor C.P. van Dam, who made a great effort in assisting me if there were any problems with the work or non work related problems during my stay in Davis. Dr. A.M. Cooperman, who did her dissertation on load control using microjets and microtabs, assisted me with everyday work related issues and with installation of the wind tunnel setup. Dr. H.J. Shiu and Dr. R. Chow often helped me out if Dr. A.M. Cooperman was unavailable. For other more general issues I could always rely on D. Richardson, staff of the Mechanical Aerospace Engineering department. Furthermore I would like to thank all the above mentioned people, and in particular Professor C.P. van Dam and Dr. A.M. Cooperman in supervising and assisting me with the work I did during my internship, because I could not have done it without their assistance and insight.

Xander Westenberg

16-01-2014

Contents

1 Introduction

The increase in size of wind turbines is a trend seen in the last years. Increasing blade size has a positive effect on the turbine efficiency, the maximum output and on maintenance costs. Obviously there are a lot of economic benefits to this. But increasing blade size will also increase the loads on the blades and the rest of the structure. The blades and the tower will need to be reinforced to withstand the higher loads, increasing material costs of the wind turbine. As an alternative load control devices can be used to minimize loads. There are several methods to apply load control on wind turbines, most well known are active pitch and variable rotational speed, another lesser known way to control loads is active aerodynamic load control. By changing the aerodynamic characteristics of the blades the lift coefficient can be changed to lower the load (the measured loads are proportional to the lift coefficient (Cooperman, 2012)).

At UC Davis aerodynamic load control is researched through the appliance of micro-tabs and microjets. In this report only the microjets are looked at. Microjets are small jets of air blown out of the airfoil perpendicular to the surface. Dr. M.L. Blaylock did a computational investigation on the application of micro-jets (COMPUTATIONAL INVESTIGATION ON THE APPLICATION OF USING MICROJETS AS ACTIVE AERODYNAMIC LOAD CONTROL FOR WIND TURBINES). Part of this research was proven in a couple of wind tunnel experiments which were part of Dr. A.M. Cooperman's research (Wind Tunnel Testing of Micro-tabs and Micro-jets for Active Load Control of Wind Turbine Blades). This research for the most part uses the same experimental setup as A.M. Cooperman, but the air supply of the microjets is redesigned.

For the air supply a 200 gallon air tank was installed, the next step was to implement a pressure and flow control device for the microjets that were to be controlled by the wind tunnel lab computer using labVIEW. In this report the process in which the setup was realized and tested is documented, describing the retailing and installation process of the experimental setup, in the final parts of the report the wind tunnel experiments are documented and the results are shown.

2 Realization of the experimental setup

In this section the companies that were contacted and what led to certain decisions regarding the experimental setup will be described. The first step that had to be done was to look for the equipment that was needed. Dr. Ir. A. Cooperman had been looking into a few options to start with, along the way some other options were found. Some turned out to be too complex, too expensive or too time consuming in the production process, which will be explained here.

McMaster-Carr

One of the options that were given was from McMaster-Carr, high flow air regulators with pressure gauge and motor-driven NPT threaded bronze butterfly valves. Because there was almost no information given on the performance of the instruments it was decided it was better to look further at other companies, described below.

Proportion Air

In my contact with Proportion Air I spoke with Melissa Gambrel about a device that could control pressure and flow speeds using labVIEW. After a few phone calls the engineering department had found a solution, a drawing is found in Figure 34 in Appendix A. The working principle was however not very clear and it was hard to say if it would work. And because it would be handmade it would take over 6 weeks to build en ship, it was also rather expansive costing over $2500.

SMCUSA

On the website of SMCUSA there were a few interesting options. They have a tool in which you can specify the dimensions and options which were available. To get pricing on some of the equipment I called SMCUSA, where I spoke to Monty Biles a sales representative, he wanted to visit us and see our setup. So an appointment was made and a few days later I showed him the setup. But the problem was that SMCUSA did not produce electronic valves larger than 1/2". We came to the conclusion there were a few options. We could use one large regulator that was mounted directly to the tank and use the old plastic manifold and use 6, 1/2" valves downstream, or build a manifold that could sustain the high pressure and downstream use multiple regulators and downstream of that six 1/2" valves.

2.1 Selection process

Before the regulator was ordered all the options were discussed in a meeting with professor van Dam and Dr. A.M. Cooperman. A clear overview of all the options that were available is seen in Table 1. The conclusion was that the options given by SMCUSA were to complex and would look for 1 1/2" valve else were, but decided to buy the 1 1/2" regulator, the SMCUSA NAR835-N14.

Table 1 Selection table

Manufacturer	Type of control	Signal used	Price	Shipping	Opinion
McMaster.com	Manual regulator 1.5” with motor driven butterfly valve 1.5”. Cycle time is 2.5 sec.	115 VAC at 60 Hz.Have screw terminals with a 1/2" conduit p ort	$688.45	Next day	Very cheap solution with not very accurate results, not much information given. Don’t know about flow characteristics
	Manual regulator 1.5” with air driven butterfly valve 1.5”. Cycle time is within 2.0 sec.	120 VAC at 60 Hz with ½” conduit port for input signal	$674.81	Next day	Faster cycle time than the motor driven.
Proportion air	Volume booster pressure control 1.5”	0-10VDC/4-20mA. 1.2 mil. Sec. step time respons	$999.5	6 weeks	Very linear V/P control. No flow control. The flow rate would be too high for PSR-B at 650 scfm
	Volume/pressure control 1.5”	0-10VDC for the flow control and also for the pressure control. 0-30psi pressure monitor	$2691	6 weeks	According to proportion air this system can modulate the flow to a max air flow at 30 psi at 150 scfm and minimum airflow is 15 scfm. Very complicated. Using 2 signals one for pressure and 1 one for flow rate.
Control air	Fairchild pressure controller ½” T90 60 0 05 06 0 N/J F E	24VDC supply, input 4-20 mA/0-10VDC	??	??	This device can only control pressure not volume
McMaster.com/thevalveshop.com	Manual regulator 1.5” with electric modulating	0-10 volt with a 24VDC electric actuator or the less expansive	$138+$2436/ $1745	Next day/1 week	V-port ball used might not be optimal for what we are using it

	ball valve 1.5” A-T controls	115VAC actuator operating time 0-90 deg =12/14 sec			for. But overall flow characteristics seem good. But have to check for linearity of the valve.
McMaster.com/thevalveshop.com	Manual regulator 1.5” with electro-pneumatic modulator ball valve 1.5” A-T controls	4-20 mA DC with a 4-20mA electro-pneumatic positioner for modulating control	$138+$1597	Next day/1 week	,,
SCMUSA	Modular regulator ½”(manual) with electro-pneumatic valve ½”	Regulator is manual DIN entry. Response 0.05s power amp. VEA250(24VDC power supply, input 0-5V	6*$38.45+6*$268.30	2013-05-07(regulator), 2013-04-29(valve)	Not much info on flow characteristics. Also this setup with 6 regulators is not ideal
	Electro-Pneumatic regulator with bracket	24VDC supply with 0-10VDC input signal	$527.75+$11.15	2013-04-29	We would have to convert this somehow. There is a second loop pressure control which needs to be converted to a volume controller.

2.1.1 Valveshop

Finding a valve that suited our application proved to be more difficult than finding a suitable regulator. For the size that was needed there were only a few options. Also manufacturers do not sell their products directly to customers, but only through retailers. An interesting options was the Valveshop, a retailer in California that sells valves for various applications. Because they are a retailer and not a manufacturer the information on their products was given by the manufacturer. Not all manufacturers present the same characterizing parameters; hence it was difficult to compare products from different manufacturers. However the Valveshop was willing to give advice on a modulating flow valve. The contact person was Bob Gates, he advised us to use an A-T Controls 60 degree v-ported ball valve with an electric actuator supplied by 115 volt alternating current (VAC) or 24 VAC. The 115 VAC model was less expansive and easier to use therefore this version was chosen.

2.1.2 Valve selection process

To check if the recommended valve would suit the microjet application a quick method for selecting valves was used. This will be described in detail below, but the main parameter in this process is the flow coefficient (Cv), which is used to select the size of a valve, or can be used to compare control valves from different manufacturers. The flow coefficient is based on a relationship between the flow rate (Q) and the square root of the specific gravity (G) multiplied by the inverse pressure drop across the valve (ΔP). It considers the flow restrictions in the valve and makes it easier to calculate the flow properties. A manufacturer finds the flow coefficient by testing the valve in a specific setup, using a standard testing method developed by the Instrument Society of America (Swagelok, 2007).

$$C_v = Q\sqrt{\frac{G}{\Delta P}}$$

The valve type that was recommended was a ball valve with a v-shaped opening, the opening size is presented by the angle α like illustrated in Figure 1. V-ported ball valves have higher accuracy than normal ball valves, when the angle α is increased the flow rate increases but the accuracy decreases. A-T Controls produced three standardized geometries to choose from; 30, 60 and 90 degree.
In the documentation on the v-ported ball valve by A-T Controls, presented in Table 2, the specific flow values for α is 30, 60 and 90 degree. Which are given for valves ranging from 1/2" to 6". In Table 2 from left to right the valve is stroked from 0% to 100%, where 0% being fully closed and 100% being fully opened. Below the table the F_L and X_t values are given for every given stroke value. F_L being the Liquid pressure recovery coefficient, which is a dimensionless coefficient that describes the pressure drop when the valve is choked. And X_t is the maximum pressure drop ratio. However these parameters are not used in the valve selection process. The 30 degree ball valve was found to be the best fit for the flow characteristics of the microjet application.

Figure 1 V-ported ball for in a valve.

Table 2 chart for V-ported ball chart of A-T Traig (TRIAG, n.d.)

"V" Series Flow Coefficients- Cv Chart

Valve Size	Ball Angle	0%	15%	20%	30%	40%	50%	60%	70%	80%	90%	100%
	30	0	0.1	0.1	0.2	0.3	0.5	0.8	1.1	1.6	2.2	2.6
1/2"	60	0	0.1	0.1	0.3	0.5	0.9	1.4	2	3.3	4.4	6
	90	0	0.1	0.2	0.4	0.6	0.9	1.5	2.2	3.8	5.4	6.9
	30	0	0.1	0.2	0.5	0.7	1.1	1.8	2.4	3.3	4.5	5.4
3/4"	60	0	0.1	0.2	0.7	1	1.7	2.8	4	6.5	9	12
	90	0	0.2	0.4	0.8	1.2	2	3.1	4.6	8	11.3	14
	30	0	0.1	0.3	0.8	1.3	2.3	3.5	5.1	9.8	8.5	10
1"	60	0	0.2	0.4	1.1	1.8	3.4	5.3	7.9	12.3	15.3	21
	90	0	0.2	0.6	1.8	3.4	5.1	8.1	11.4	16	21	29
	30	0	0.2	0.4	1.1	2	3.7	5.5	8	10	13	15
1 1/4"	60	0	0.2	0.6	1.8	3	5.5	9.5	12.8	19	26	39
	90	0	0.3	0.8	2	5	8	14	19	28	39	55
	30	0	0.3	0.6	1.6	3	5	7.5	11	14	17	20
1 1/2"	60	0	0.4	0.8	2.5	4	8	13	19	27	40	52
	90	0	0.4	0.9	3.5	7	13	20	31	42	63	78
	30	**0**	**0.4**	**1.2**	**3.8**	**6**	**10**	**15**	**23**	**31**	**43**	**60**
2"	60	0	0.4	1.5	4.6	9	16.5	27	39	55	83	110
	90	0	0.5	2	6	12	22	35	45	70	105	135
	30	0	0.4	1	4	8	12	18	28	37	62	75
2 1/2"	60	0	0.4	1.5	5	10	21	34	53	75	103	150
	90	0	0.5	1.7	7	14	28	48	70	106	160	218
	30	0	0.5	1.2	4	8	14	23	33	46	65	82
3"	60	0	0.5	2.5	6	14	25	40	65	91	128	165
	90	0	0.7	3.5	8	18	35	60	90	135	205	310
	30	0	0.6	2	6	15	29	48	71	100	130	159
4"	**60**	**0**	**0.7**	**3**	**11**	**25**	**40**	**59**	**90**	**141**	**212**	**356**
	90	0	1	3.5	16	40	75	125	190	295	442	670
	30	0	0.9	3.2	14	33	60	103	155	220	280	350
6"	60	0	2	5	22	60	110	190	285	416	586	800
	90	0	3	8	35	90	160	280	425	650	970	1480
F_L		0	0.96	0.95	0.94	0.93	0.92	0.9	0.88	0.86	0.82	0.75
Xt		0	0.98	0.77	0.71	0.67	0.64	0.63	0.62	0.55	0.43	0.4

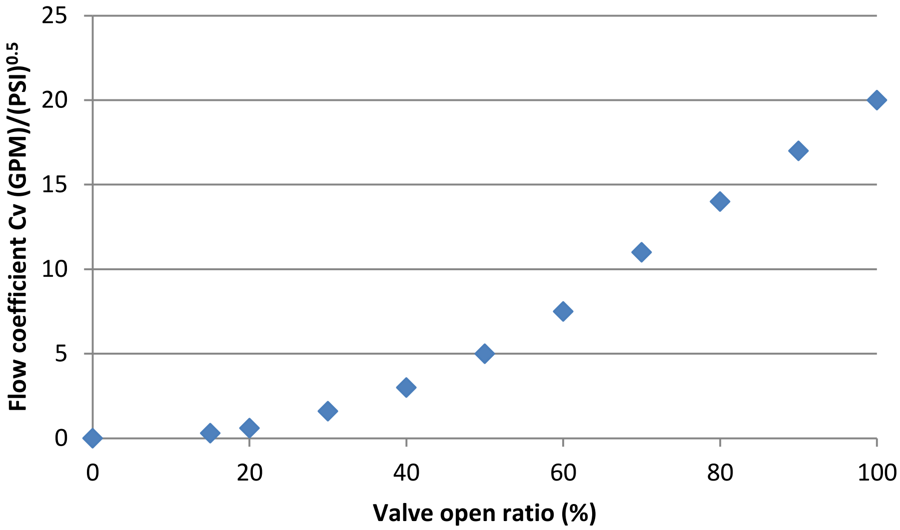

Figure 2 Flow coeficient

For selection and sizing of a valve there are a few things to look at and they are described in the list below (Haslego, 2011). However there were some troubling issues with this. For instance there was no data on the pressure loss in the system and besides this there was no well defined operational flow rate so an educated guess had to be made. Also the process described by (Haslego, 2011) is for valve controlling a liquid stream. For high flow rate pneumatic systems compressibility has to be considered. However at 120 SCFM the speed is 25 m/s which is far below 0.3 times the speed of sound and therefore the air can be considered incompressible.

1. Determine the system: flow characteristics (Maximum flow rate, operation flow rate and minimum flow rate), total pressure drop (30 PSI), the medium (Air), temperature (70° F), pressure and specific density (1 for air)
2. Determine the maximum allowable pressure drop (rule of thumb says 10 PSI is reasonable (Haslego, 2011)).
3. Calculate the flow characteristics ($C_v = Q\sqrt{\frac{G}{\Delta P}}$), Q = design flow rate(SCFM), G = specific gravity relative to air (1 by definition) and ΔP is the allowable pressure drop across a wide open valve(PSID).
4. Preliminary valve selection: avoid using the lower 10% and upper 20%, stay between 10% and 80% of the valve stroke.
5. Check the gain across applicable flow rates. The gain is defined as the change in flow divided by the change in stroke, by rule of thumb the difference between the gains should be lesser than 50% of the highest gain. If this value is too high the sensitivity of the control valve will be too high, causing difficulties in controlling the flow rate carefully.
6. Table 3 the flow rates and stroke values are defined, the change in flow rate and stroke and the gain are given in Table 4.

Table 3 Flow parameters

	Flow (SCFM)	Flow (GPM)	Cv ((GPM)/(PSI)$^{0.5}$)	Stroke (%)
Minimum	20	150	1.08	24.8
Operation	80	598	4.38	46.9
Maximum	150	1122	8.13	61.8

Table 4 Change in flow rates and stroke also the gain is given.

	Change in flowrate (GPM)	Change in stroke (%)	Gain (delta flow (GPM) /delta stroke (%))
Operation - minimum	448 (3.3)	22.1	20.27
Maximum - operation	524 (3.75)	14.9	23.71

The difference between the gain values is lower than 50% of the higher value: 23.71 - 20.27 = 3.44. Also the gain should never be lower than 0.5, which is true in this case. Therefore the valve should be well fitted for this flow application.

2.2 Issues with The valve shop and A-T control

In the initial contact with the valve shop I looked at two different valve actuator types, the Electric and Electro-Pneumatic type. Because using an electrical power supply is easier than supplying power pneumatically the preference was for the electrical system. Initially it was thought that the stroke time of both systems were about the same. In the specification sheet there were several different systems explained, for some of those systems a difference was listed for a 50 or 60 hertz power supply for others only 50 or 60 hertz was listed. When bot 50 and 60 hertz were listed the values would be in the same cell but segregated by a dash, this was misunderstood by me for a fraction because all the other values round figures.
Besides having contact with Bob Gates at the valve shop there was also contact with A-T controls to get a second opinion. In this conversation various things where mentioned including that the stroke time was under one second. There must have been some misunderstanding as they agreed on this.

2.3 New actuator with positioner from Process Instruments

Eventually it was decided that a replacement valve was needed. The Valve Shop did not take back the electric actuator with servo card because the servo card was used when the valve was tested with labVIEW at the wind tunnel facility. They offered a refund of 40% of the retail price if we bought a replacement part for full price. It was decided it would be best to look for an electro-pneumatic actuator with a positioner elsewhere.

M. Czasnojc from Process Instruments was willing to sell the electro-pneumatic actuator with positioner with 100 dollar discount for 1150. According to him it would work with 80 PSI shop air, however if the pressure would drop it might cycle slower or stop. To be certain the electro-pneumatic actuator with positioner met the specs Martin Czasnojc took a look at the windtunnel with the microjet setup. To be absolutely certain everything would fit, Dr. Cooperman helped with studying the technical drawings. Eventually we came to the conclusion that it would work and Dr. Cooperman put in the order.

3 Test section

Here the test section is described, consisting of the windtunnel, the modified S819 airfoil with the microjets installed and the air supply installation with the regulator and electric valve. The electropneumatic actuator with positioner is also explained at the end of this section.

3.1 Windtunnel

The UC Davis Aeronautical Wind Tunnel used for the experiments is an open circuit wind tunnel manufactured by Aerolab. An example of the wind tunnel can be seen in Figure 3. The fan sucks the air from the left of the wind tunnel through the honey comb and four screens to minimize turbulence. The taper ratio of the inlet to the test section is 7.5:1. The test section dimensions are 33.6 in. (0.85 m) high, 48 in. (1.2 m) wide and 12 ft. (3.7 m) long. In the test sections are two turn tables and a pitot tube that can be positioned with a traversing mechanism.

Downstream of the test section the diffuser is found. The purpose of the diffuser is slow down the air and recover pressure from the kinetic energy to reduce the power needed for the propeller.

At the end the Fan and Silencer are found. The silencer reduces the aero acoustic disturbances in the flow. The fan is powered by a 125 hp Alternating current motor. The electric controller has a repeatability of 0.2% of full scale resulting in a 0.64% uncertainty in the determination of the Reynolds number (Cooperman, 2012).

The balance can measure force in lift direction up to 150 lbs, drag up to 50 lbs and the pitching moment can be measured up to 50-ft lbs. The accuracy of measurement is 0.1% of full scale of each different component. Because we are using a two dimensional model (there is no wing tip and the cross section of the airfoil is constant) the lift measured is registered in the data as side force, the angle of attack is registered as ψ. But in the report this will be referred to as lift L and angle of attack α.

The design of the wind tunnel is well suited for the application and can quickly increase or decrease the air velocity to model gusts. Also the pressure vessel size only supplies compressed air for only approximately 20 seconds. High ramp up or down speeds make sure that that testing time can be minimized so there is enough compressed air to maintain test conditions constant for the period of time needed to simulate a gust.

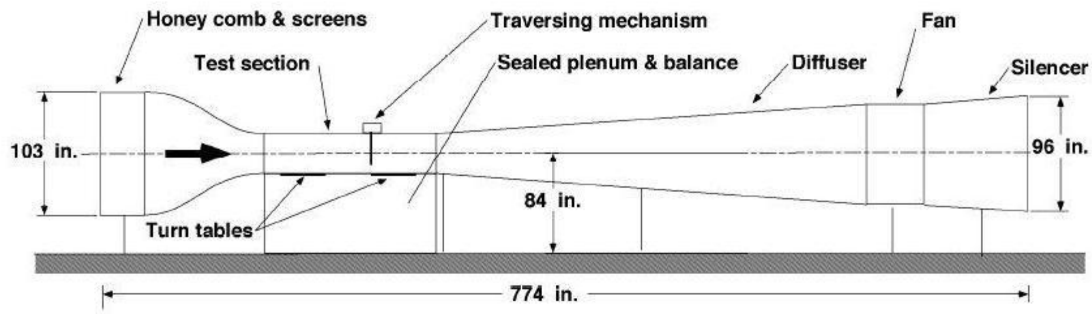

Figure 3 UC Davis Aeronautical Wind Tunnel (Cooperman, 2012).

3.2 Airfoil

The airfoil used, for testing of the micro-jets, is a modified S819 profile, the tail section has been thickened to make room for the micro-jet plenums. A comparison of the S819 and the profile used for testing can be seen in Figure 4. As can be seen in the picture the profile is thickened from mid chord towards the trailing edge. At 95% chord length the thickness is doubled, this is the position where the lower surface microjets positioned. In Table 5 all the parameters that concern the airfoil can be found.

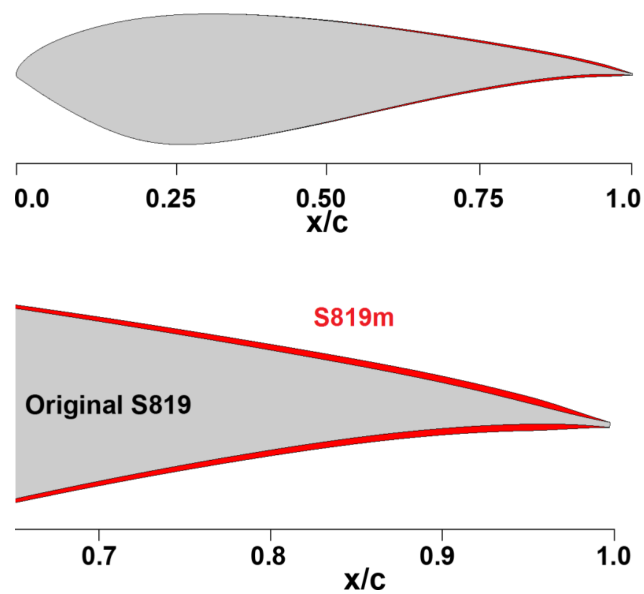

Figure 4 Comparison of original S819 airfoil compared to the one used by UC Davis.

The span of the blade is build out of six identical pieces, closed off by a bottom and a ceiling cap. The 6 airfoil pieces are connected to each other using little alignment pins that are fitted into on the airfoil piece next to it. For each individual airfoil piece the holes are located on the bottom side of the airfoil, at the same place at the top side of the airfoil piece the notches are found. This way when the airfoil pieces are put together they will be aligned. All pieces are hold together using two steel treaded support rods fastened with nuts on the bottom and ceiling side of the blade. Each airfoil piece is 5.36 in (136 millimeter) wide and consists out of a body and a tail connected with a dovetail joint, the joint is located at 53% chord for both the pressure and suction surface. In the sides of the body there are three holes for the alignment pins. This is illustrated in Figure 5. However this particular picture is for the micotab system, therefore disregard the linear actuators and tabs.

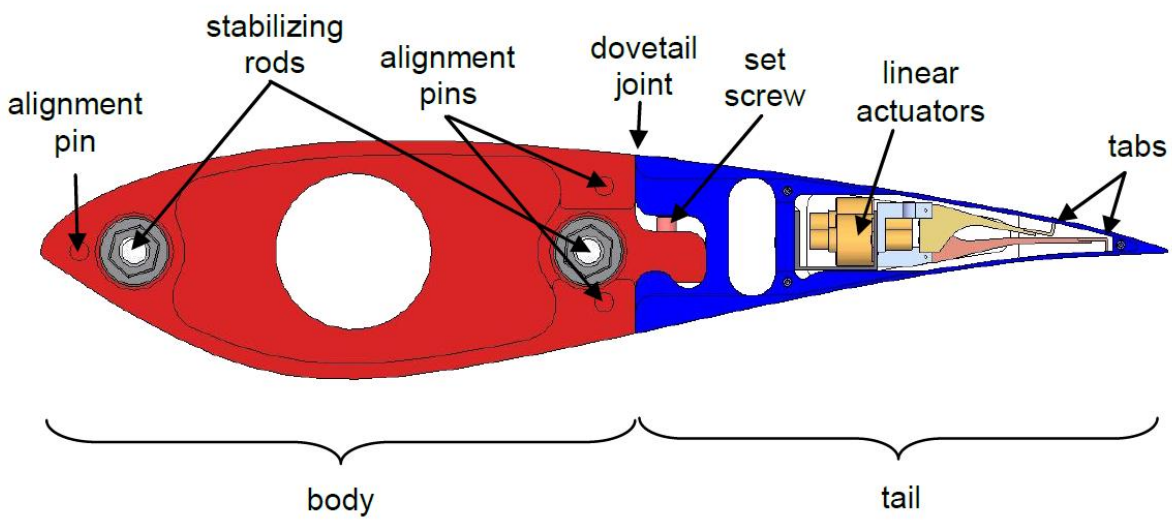

Figure 5 Cross section of a airfoil piece with microtab system.

There is a large round opening in the ceiling cap for the hoses to supply the air to the plenums. The hoses are fed through a hole in the top of the wind tunnel testsection. The bottom cap is connected to the blade pieces through the steel treaded support rods by two nuts. The fitting and opening can be seen in Figure 6. The placement of the plenums inside the hollow blade can be seen in Figure 7.

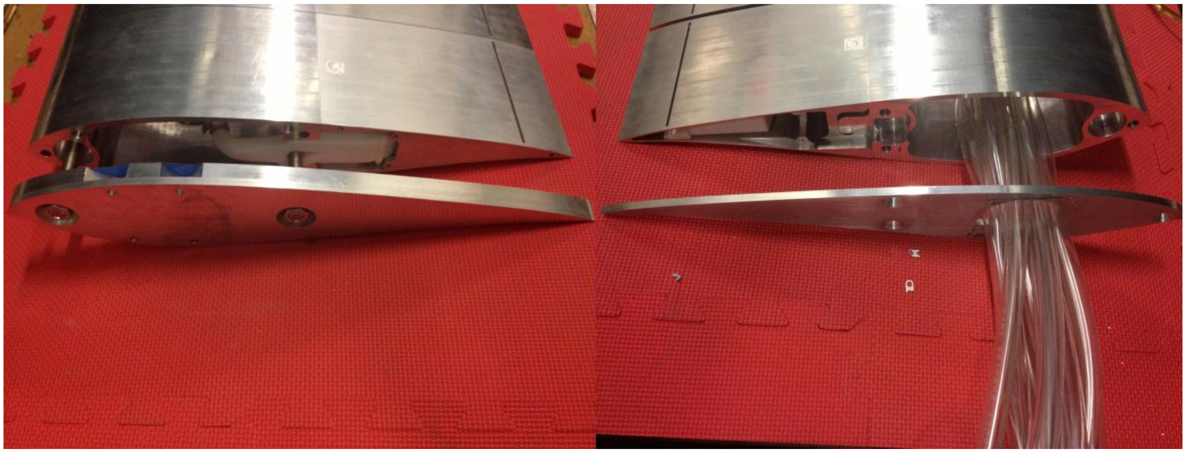

Figure 6 Left the bottom cap with fitting of the nuts, on the right the ceiling cap with opening for tubing.

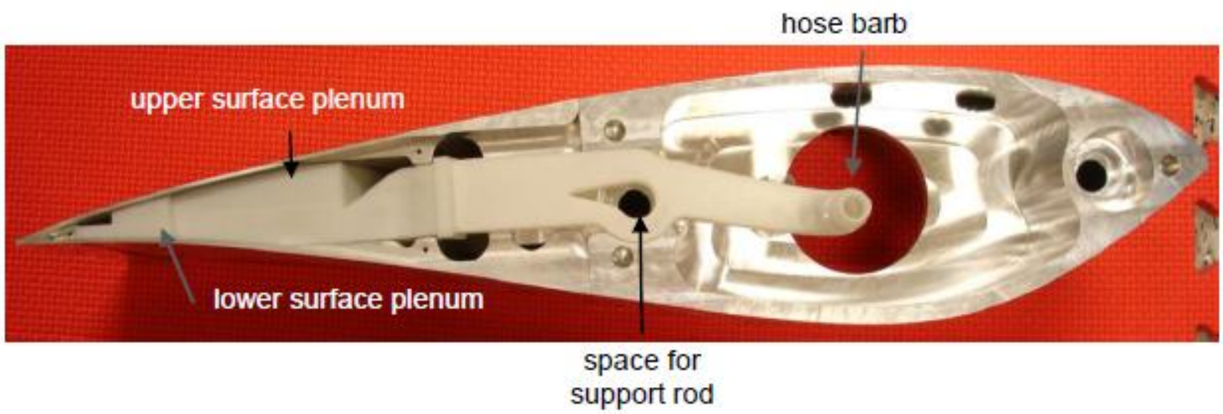

Figure 7 Single section of the model with the lower micro-jet plenum installed.

Table 5 Physical parameters of the modified s819 model used to fit the microjet plenums.

Element	Amount
Chord	18 in. (457 mm)
Span	
With end caps	33 1/8 in. (841 mm)
Without end caps	32 1/8 in. (816 m)
Joint location of body and tail	53% chord
Maximum thickness	3.8 in. (96 mm) at 21% chord
Material	6061 aluminum
Weight, complete model with hollow tails with jet assembly	66 lbs (29.93 kg)
Slot location	
Upper surface	90% chord
Lower surface	95% chord
Slot	
Width	0.09 in. (2.3 mm)
Length	5.1 in. (120 mm)
Gabs between slots	0.26 in. (6.6 mm)

3.3 Microjet assembly

3.3.1 Plenums

The micro-jets are located at 90% chord on the suction side surface and at 95% chord on the pressure side surface. They are 0.09 inch (2.29 millimeter) wide and 5.1 inch (129.54 millimeter) long in span wise direction. The plenums are designed to use as much as possible of the available space in the model. An example of one of the pieces with the pressure and suction side plenums in place can be seen in Figure 7. Most of the dimensions were already mentioned but can also be found in Table 5.

The plenums have a 0.435 inch (11.05 millimeter) opening, which is referred to as the hose barb, which connects them to the air tubing. From there on the cross section keeps increasing up until the outflow point of the plenum, this is done to minimize energy losses. There are six plenums for the pressure side jets and 6 plenums for suction side jets. With increase of lift the jets on the suction side will be used and when the lift decreases the jets on the pressure side will be used to compensate the loads on the blade. Eventually in a later stadium of the research upstream of the plenums there will be a switch to choose between the pressure or suction side jets. Two manifolds will be used to split the large stream of air (one and a half inch) into twelve, half inch tubes connecting the suction or pressure side jets. The manifold used can be seen in Figure 8.

Figure 8 Manifold connecting six micro-jets (1.5 inch inlet on the right and 6, 0.5 outlets for the microjets on the left)

Pressurized tank and regulator

Outside the wind tunnel the air supply is found: a 200 gallon air tank that will be pressurized up to 80 PSI. The tank is manufactured by Manchester Tank (LB, n.d.), it can be seen in Figure 9 on the right. The tank has connections ranging from 0.25 inch to 2 inch, the opening on top of the tank was used to attach a pressure gauge and on the bottom a drain can be found. The tank is filled with a shop air installation that delivers air at 80 psi using a 0.5 inch quick release connector on the lower front side of the tank like seen on the right side in Figure 9. The outflow of the tank uses a 1.5 inch NPT connection; here the regulator and electronic valve are connected to regulate the pressure and the flow amount. The regulator can be seen on the left in Figure 9. The knob on top of the regulator is used to set the pressure and on the back of the regulator a gauge is found, this can be seen in the picture of the tank when looked closely. Between the regulator and the tank there is a manual valve with a large yellow handle to open or close it as an extra safety feature. There is also a safety relief valve on the right side of the tank (between the tank and the wind tunnel) that is rated to 150 PSI.

Figure 9 Left: SMCUSA NAR 835-N14G, Right: Manchester Tank with regulator attached.

Table 6 Physical parameters pressurized air tank.

Property	Amount
Size (H,D)	80 in. x 30 in.
Volume(V)	200 Gal. (757 L)
Max Pressure(P_{max})	200 PSI (1378 kPa)
Weight	450 lb (204 kg)

Using the ideal gas law the maximum flow time can be calculated. All physical parameters for the pressurized air tank can be found in Table 6. At 80 PSI the tank contains n_{high} mol air. All variables can be found in Table 7.

$$P_{\text{high}}V = n_{\text{high}}RT \rightarrow n_{\text{high}} = \frac{P_{\text{high}}V}{RT} = 169\ \text{mol}$$

Table 7 Variables concerning the air pressure tank.

Variable	Amount
High pressure (P_{high})	80 PSI (551 kPa)
Low pressure (P_{low})	15 PSI (103 kPa)
Molar mass air (m_{Air}) (Anon., 2013)	0.06384 lbs.mol^{-1} (0.02896 kg.mol^{-1})
Volume tank (V)	200 Gal (0.757 m^3)
Temperature (T)	75 F (297 K)
Universal gas constant (R)	8.31 J.K^{-1}.mol^{-1}

The micro-jets are supplied with air at 15 PSI pressure measured at the regulator. Therefore the pressure in the tank cannot drop below 15 PSI. At 15 PSI there is still n_{low} mol of air left in the tank.

$$P_{\text{low}}V = n_{\text{low}}RT \rightarrow n_{\text{low}} = \frac{P_{\text{low}}V}{RT} = 32\ \text{mol}$$

Therefore there is at the maximum $n_{\text{high}} - n_{\text{low}} = n_{\text{max}} = 140\ \text{mol}$ of air that can be used. At full capacity the micro-jets use 125 SQFM of air (Cooperman, 2012). The density is assumed to drop linearly when the tank is emptied. The average density (ρ_{avg}) can be calculated with the perfect gas law when the pressure drop is known.

$$P = \rho RT \rightarrow\ \rho_{avg} = \frac{P}{RT} = 0.02431\ \text{lb.}\,\text{ft}^{-3}(3.895\ \text{kg.}\,\text{m}^{-3})$$

Now the mass flow can be calculated using $\dot{m} = Q.\rho_{\text{avg}}$, considering that Q = 125 SCFM (0.05899 m^3/s) the mass flow $\dot{m}$ = 0.5066 lb/s (0.2298 kg/s) or 7.935 mol.min^{-1}.With this it can be calculated that it takes 17.64 seconds for the tank to drop from 80 PSI to 15 PSI pressure at a flow rate of 125 SCFM.

3.4 Modulating valve

3.4.1 Electric actuator/digital positioner

The electric actuator and servo card together are called a WED-500, it is build by A-T controls and is advertised to be used with ball valves. Below the features of a standard WE-500 actuator are stated, a picture of it can be seen in Figure 10(TRIAG, n.d.).

1. Compact and light due to high grade aluminum alloy housing.
2. High resistance to corrosion due to hard anodizing on inside and outside with polyester powder coating on external surface.
3. Output torque: 530 In-lbs.
4. The actuator motor is a reversible, high torque and low current design.
5. Weatherproof (IP67, NEMA 4, 4X)
6. Position indicator on top.

Figure 10 WE-500 actuator

The model we used was setup to be powered by a 110V AC source, this was the most cost efficient option and is also easiest to use because no adapter was needed. The performance can be seen in Table 8.

Table 8 WE-500 performance

Type (model)	**Maximum Output Torque**	**Operating Time 60/50 Hz**	**Mountin g Size**	**Full Load Amps**			**Locked Rotor Amps**			**Duty Cycle**	**Number of Handle Turns**	**Weight**
				AC 1PH. 50/60Hz		AC/DC	AC 1PH. 50/60Hz		AC/DC			
	In-Lbs.	90°	ISO5211	110V	220V	24V	110V	220V	24V	S2	N	Lbs.
WE-500	530	12 or 14 seconds	F03/F05 /F07	0.4	0.2	0.8	0.5	0.25	2.5	70%	8	6.61

The electronic positioner or servo card used is a TDC100 and is bolted onto the actuator. It has a resolution of 450 points for a quarter turn. For control It has a 3 button layout and can be configured for various command types: 4-20mA, 1-5VDC, 0-5VDC and 0-10VDC. The last option is the one used. The features quoted by (TRIAG, n.d.) are:

1. Positions to ±0.1° with quarter-turn actuators ranging from 2 sec to 120 sec (with or without a brake).
2. Adaptive Control feature continuously adjusts for load and actuator conditions and eliminates calibration procedures and auto-cal operations.
3. Three button control provides easy setup and eliminates the need for instrumentation.
4. Polarity Detection feature allows direct or reverse acting operation without re-wiring.
5. Electronic Brake feature can eliminate need for a mechanical brake in many applications, and extends mechanical brake life when used.
6. Stall Detection feature protects actuator motor from a stall condition.
7. Automatic Duty Cycle Control feature prevents shutdown of a process due to a thermal overload of the actuator motor, and allows actuators rated for 25% duty or more to be safely used.
8. Operating temperature range of 0 to 60°C.

The installation is clearly described in the operation and maintenance manual of A-T control. But the actuator and electric positioner were already assembled when it was received. Only the signal and power wires needed to be installed. The outline of the TDC 100 is given in Figure 11, it is clear that the signal wire needs to be connected to terminal J2 for line 4 and 6, and the power cable needs to be connected to terminal J2 for lines 1, 2 and 3.

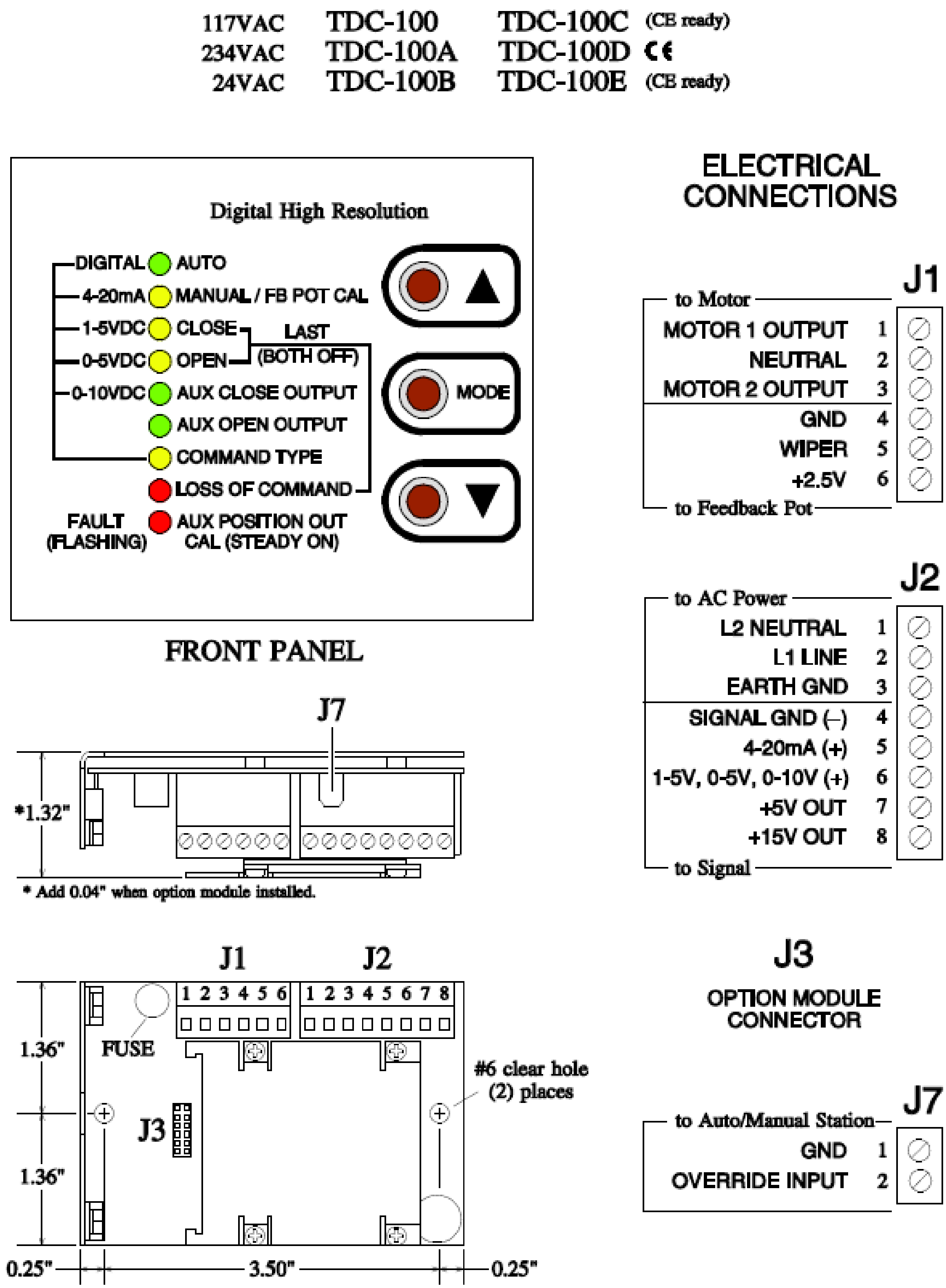

Figure 11 Outline of the TDC100 117 VAC (TRIAG, n.d.)

3.4.2 Electo-pneumatic actuator with positioner

The electro-pneumatic actuator with positioner, shown in Figure 12, is also manufactured by A-T controls. The package is build out of 2 different elements: the 2R130DA double acting air actuator and the Rotary Type EPR1000 positioner controlled by a 4-20 mA signal and powered by 80 PSI compressed air. The output characteristics are linear. Most important parameters can be found in Table 9.

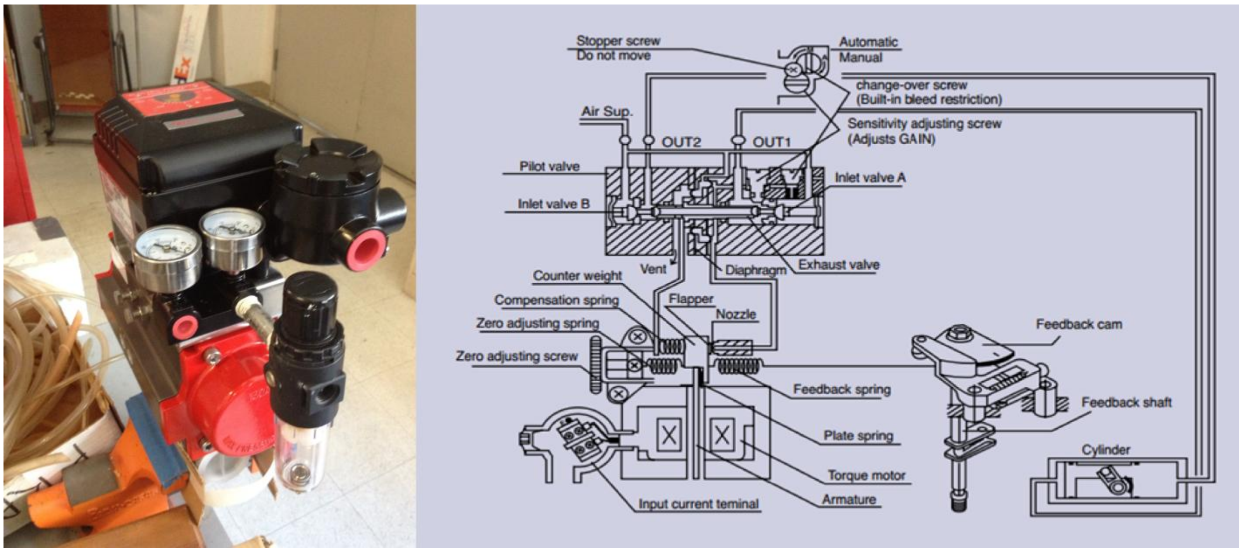

Figure 12 Photo of the electro pnuematic actuator/positioner attached to the valve and a schematic representation of the EPR1000 (TRIAC, n.d.).

A schematic representation of the positioner can be seen on the right in Figure 12. When the current to the positioner increases, the armature will be rotating in counter clockwise direction, moving the counterweight to the left. This will increase the clearance distance between the flapper and the nozzle, causing the nozzle backpressure to decrease. Because of this the exhaust valve of the pilot valve moves to the right, and the output pressure of the of OUT 1 increases as output pressure OUT 2 decreases (TRIAC, n.d.). A schematic representation of the actuator is seen in Figure 13. The output channels of the positioner are connected to port A and B of the double acting actuator. When the air pressure supplied to port A is increased the pistons are forced away from each other, this then rotates the drive pinion counterclockwise. When the air pressure to port B is increased the pistons are forced together and the pinion will rotate in clockwise direction.

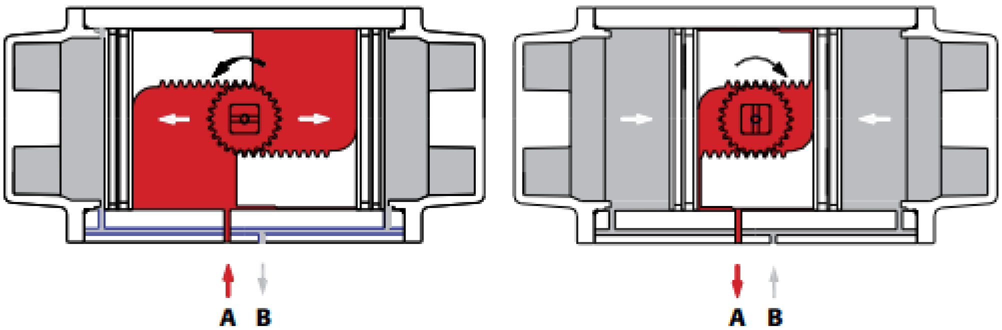

Figure 13 Double acting actuator (TRIAG, 2012).

Table 9 Characteristic parameters of A-T controls modulating valve.

Characteristic parameter	Amount
V-ported valve Valve used	A-T Controls V8C-TS-150/2R4D-EX-6
Specific flow constant range (Cv)	0-20
Stroke range 20 to 125 SCFM	21.8% - 64.8%
Double acting actuator used	A-T Controls 2R130DA actuator
Double acting torque	1054 (in-Lbs)
Cycle Times (seconds per 90 Deg’s)	1.2 sec.
Positioner used	A-T Controls EPR1000
Input signal	2-20 mA DC
Input Resistance	235±15Ω
Supply pressure	80 PSI
Linearity	Within ±1.5% Full Scale
Sensitivity	Within 0.5% Full Scale
Hysteresis	Within ±1.0% Full Scale
Repeatability	Within ±0.5% Full Scale

3.5 Sensors used

3.5.1 Flow meter

The flow rate through the microjet plenums is measured using a Foxboro vortex flow meter(Model #84-U1HS1SSTJF). Inside the piping of the flow meter there is a shedder bar in the centre, It measures the frequency of the shredding vortex. When the Strouhal number is known the stream velocity can be evaluated using the following formula: $S = \frac{nD}{U_\infty}$. Here *n* is the frequency, *D* the pipe diameter, U_∞ the stream velocity and *S* the Strouhal number. The Strouhal number is dependent on the Reynolds number, the relationship can be seen in Figure 14. Even for the lowest flow rate of 20 SCFM the Reynolds number is well above 10^3, therefore the Strouhal number is constant and the velocity can be determined.

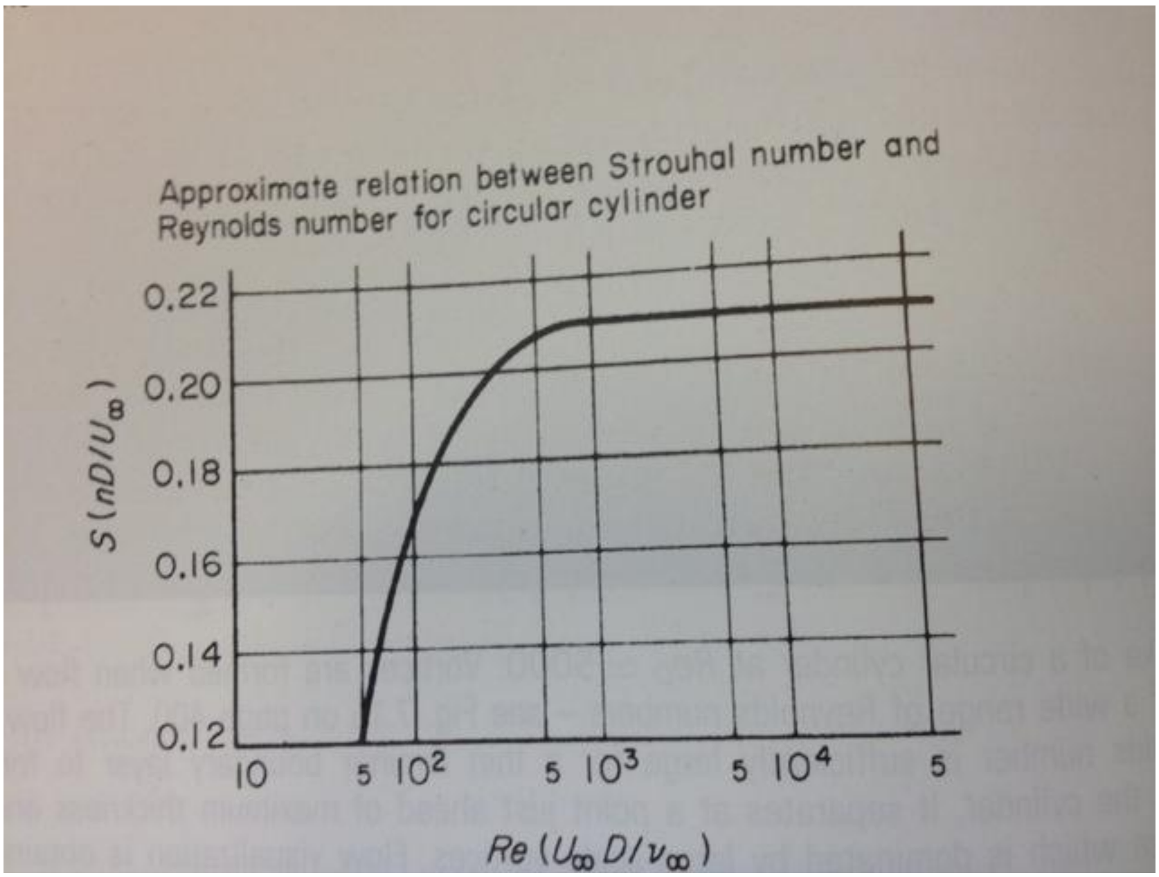

Figure 14 Relation between the Strouhal and the Reynolds number.

3.5.2 Pressure Measurement

There are two fast pressure transducers installed on the airfoil. The piezoresistive transducers are manufactured by Endevco (model 8507c-1), a four-arm strain gauge bridge diffused into a sculptured silicon diaphragm, specifications can be found in

Table 10. The full scale output of the transducer is approximately 230 mV. The signal is amplified using an Endevco VDC amplifier (model 136), increasing the full scale output at 1 PSI to 5V. The amplifier conditions the signal using a low-pass filter, specifications are found in

Table 10. The low-pass filter is used so that the frequency response is maintained below 11 kHz because of the resonant frequency of the diaphragm at 55 kHz.

Table 10 Endevco transducer and amplifier specifications.

Description	Specifications
Transducer diaphragm resonant frequency	55 kHz, allowing freq. respons of 11 kHz
Transducer range differential	-1 to 1 PSI (±6.89 kPa)
Transducer combined uncertainty (non-linearity, hysteresis and non-repeatability) for FPT1 (serial number 10355)	0.0110 PSI
Transducer combined uncertainty (non-linearity, hysteresis and non-repeatability) for FPT2 serial number 10241)	0.0147 PSI
Transducer change in sensitivity due to temperature changes for FPT1 across temperature range of 0° F to 200° F (-18° C to 93° C)	3.26%
Transducer change in sensitivity due to temperature changes for FPT2 across temperature range of 0° F to 200° F (-18° C to 93° C)	2.44%
Amplifier low-pass filter gain	-3 dB
Amplifier low-pass filter phase (corner frequency)	10 kHz

The fast pressure transducers are installed below the surface of the airfoil directing into the airfoil. In the surface of the airfoil there are small orifices. The orifices have a diameter of 0.031 inch (0.78 millimeter). Metal tubes with an outer diameter (OD) of 0.028 inch (0.71 millimeter) are press-fit into the orifices extending into the airfoil for 0.2 in. (5.08 millimeter). The orifices with the metal tubes attached are referred to as pressure tabs, these where initially used to connect hoses for static pressure measurement in research for microtab (Cooperman, 2012) load control but are now used to support the fast pressure transducers. In total there are 41 pressure tabs, to get an idea how this looks like study Figure 15. Obviously the location fast pressure transducers cannot be changed during testing, therefore a single location has to be chosen. At $x/c = 0.125$ (x denotes the position along the chord c starting at 0, the leading edge of the airfoil, and maximizes at $x = c$, at the trailing edge) the pressure difference gives a good representation of the change in lift (M. Gaunaa, 2009). However at this precise location there is no pressure tab installed, therefore the closest pressure tab was chosen, which is located at $x/c = 0.15$.

Figure 15 Section with pressure tabs on the top and bottom surface.

The transducers size is preferably small so it fits into the airfoil, hence there also is only a small distance between the surface and the point of measurement. The shape of the transducers is cylindrical, with the measurement diaphragm on one side and the venting tube and electric wire for the signal on the other side. To fit the tubing into the metal pressure tabs a smaller diameter tube is glued into the tubing with the transducer inside it. A visual representation is found in Figure 16, tubing sizes can be found in Table 11.

Table 11 Tubing sizes

Description of tubing		Size
Tubing to hold transducer inner diameter (ID)		3/32 in. (2.38 mm)
Tubing to fit onto metal pressure tabs, and into 3/32 in. ID tubing on the other end.	ID	1/32in. (0.71 mm)
	OD	3/32 in. (2.38 mm)

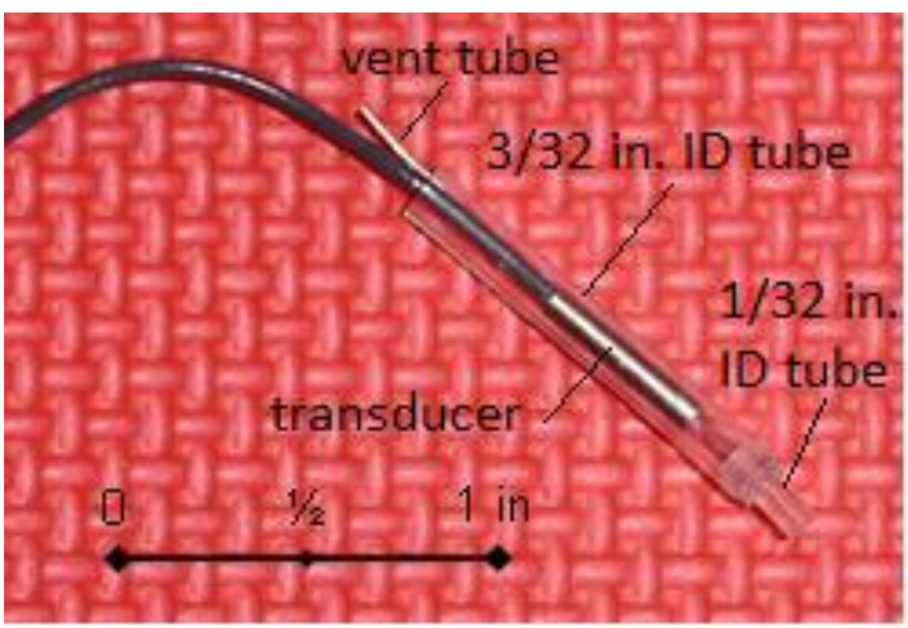

Figure 16 transducer with Tygon tubing, ready to install onto metal pressure tabs (Cooperman, 2012).

4 Building the setup

Here the installation of the model with all its facets will be described. This involves the installation of the model, calibration of the tunnel equipment and the general procedure that is involved with running the wind tunnel experiment.

4.1 Installation of the model

As explained earlier the airfoil exists out of six sections and a bottom and ceiling cap, all kept together by two alignment pins. All the plenums, for the upper and lower surface jets, were already installed and connected to the tubing at an earlier time. The tubing was directed to the top of the airfoil through the ceiling cap like seen on the right side of Figure 6.

Installing the fast pressure transducers

The fast pressure transducers were recalibrated after they were used last time. Therefore they needed to be rewired, because the wire was too short to be connected to the analog-to-digital converter (ADC). The soldering process can be seen in Figure 17. After this the separate wires were isolated and a larger piece of tubing was put over all the wires to increase the robustness. Finally the wiring needed to be pulled through the opening in the ceiling cap towards mid of the span through the tubing that was already in place.

The fast pressure transducer was fastened on to an Electrical wire to guide it towards mid span between the tubing. When it was in the mid of span it was connected to one of the pressure tabs, more on this will be explained in the section Data acquisition.

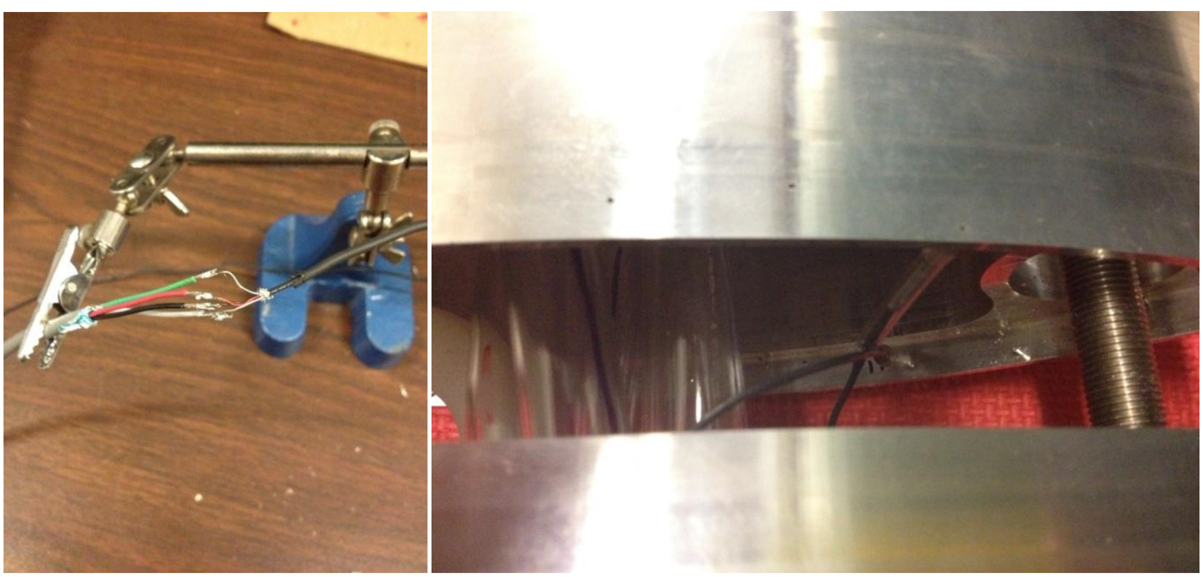

Figure 17 Soldering of the transducer wiring (left), Installation of the pressure transducers on the pressure tabs (right).

Putting the model in the windtunnel

Because the model was quite heavy the airfoil was put in the test section of the wind tunnel with 3 persons, 2 persons on each side of the test section and 1 person on top of the wind tunnel to support the tubing and wiring of the fast pressure transducers.

Before the model was put inside, the wind tunnel test section the seat was installed. The forces and moments were closely monitored to make sure that the applied torque did not surpass the load limits of the balance, which are specified in Table 12.

Table 12 Load limits of the balance and measurement system

Property	Limit
Lift	±300 lb
Drag	±50 lb
Side Force	±150 lb
Pitching Moment	±70 ft-lb
Rolling Moment	±50ft-lb
Yawwing Moment	50ft-lb
Angle of Attack	±35˚
Angle of Jaw	±45˚

The airfoil was secured with 4 screws inserted in 4 notches in the bottom cap like seen in Figure 6 on the left. The notches were taped over later to ensure the flow was not disturbed. The tubing and fast pressure transducer wiring that were coming out of the ceiling of the airfoil was fed through a hole in the top of the wind tunnel test section. The fast pressure transducer wiring was connected to the Endevco VDC amplifier that was already calibrated. The VDC amplifier was in turn connected to a connector block which acts as an interface between the sensors and the National Instruments (NI) Data Acquisition (DAQ) card in the pc, the data flow is depicted in Figure 18.

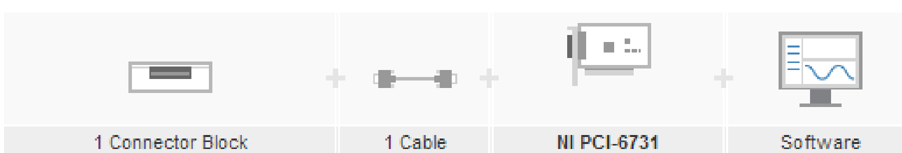

Figure 18 Connection scheme NI hardware (www.ni.com)

4.2 Tubing and connection of the Foxboro vortex flow meter

The tubing connected to the jets is fed to the manifold, here six 0.5 in. tubes are combined into one large 1.5 in. tube. The 1.5 in. tube is then connected to the Foxboro vortex flow meter, this can be seen in Figure 19. Due to time limitations the flow meter was constrained with a rather half-baked solution using climbing rope. A more permanent solution would be to use 2 c-rails and a set of clamps. The c-rails could be fastened onto a metal plate which could be screwed in the holes that are on each side of the top plate of the wind tunnel test section the same holes are used to secure the pitot tube positioning mechanism. In Figure 19 the white tubing goes towards the air tank and is connected to the electric valve, the transparent tubing leads towards the jets and is connected to the manifold.

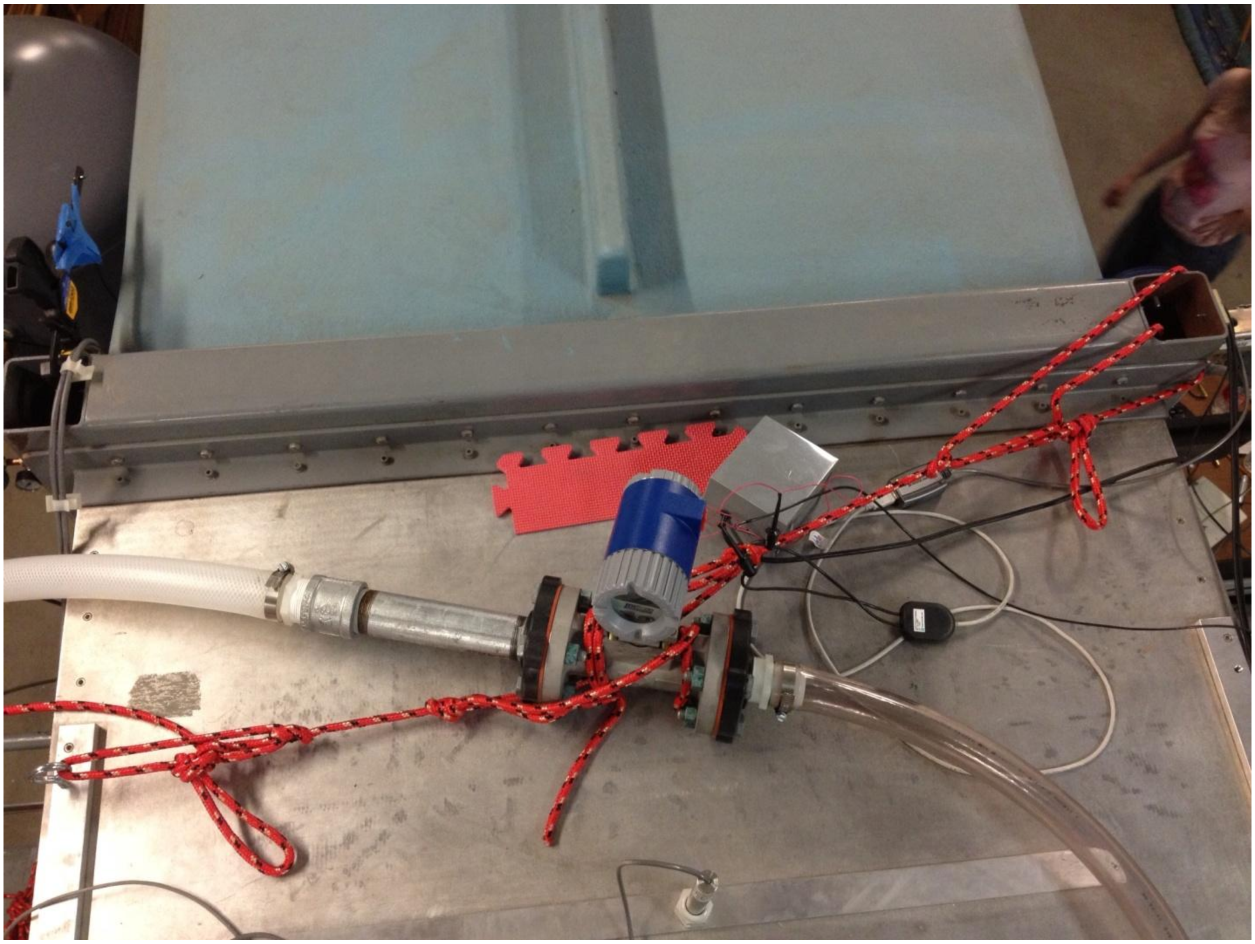

Figure 19 Topside view of the windtunnel at the beginning of the test section, showing how the vortex flow meter was installed during testing.

4.3 Calibrating the turntable

After the model was installed and the tubing connected, the turn table was calibrated. In ideal cases this needs to be redone before every test, but in this case it was done only before major changes in the setup were made, like when switching from the suction side jets to the pressure side jets.
In the calibration process the turntable is set to zero by aligning the turntable with the zero marking on the wind tunnel floor and repeating this for all even numbered angles of attack. This was done up to 20 degrees angle of attack. When 20 degrees was reached the table was turned in the other direction and again for all even angles of attack down to -20 degrees angle of attack the turn table was aligned with the markings on the tunnel floor. For each angle of attack a voltage is given, this way a correlation between the angle of attack and voltage that the turntable sensor is supplying to labVIEW is found.

4.4 Setup of the 4-20 mA Current Loop

The Foxboro vortex flow meter outputs a 4 to 20 milliampere (mA) at a constant 24 volt direct current (VDC) depending on the flow speed. This is often used for industrial equipment because voltage based transducers suffer from voltage drop over large distances. But the National instrument DAQ only reads 0-10 VDC signals.

The working principle of a 4 to 20 mA current loop wil be explained now. A 24 VDC power supply is setup in series with the flow meter to power the system, the flow meter regulates the current between 4 mA when there is no flow and 20 mA for the max flow rate.The current signal can be measured by placing a shunt resistor between the leads of the connector box (like seen in Figure 20), to convert the current signal into a voltage signal.

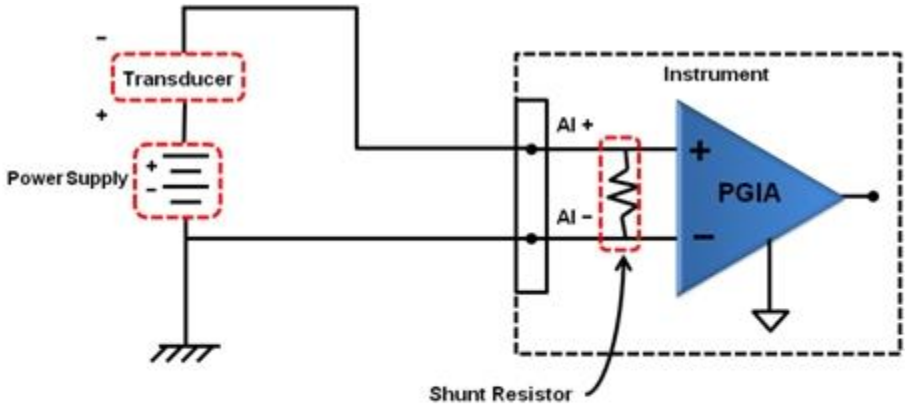

Figure 20 Current loop (From National Instrument Website)

4.5 Installation of the valve

Information on wiring the TDC-100 servo card and the WED-500 electric actuator with the NI DAQ equipment can be found on the A-T controls website. However most was preinstalled when it was received only the power cables and the signal cables needed to be connected. This was done as is described in Electric actuator/digital positioner, the result with all the wires installed can be seen in Figure 21.

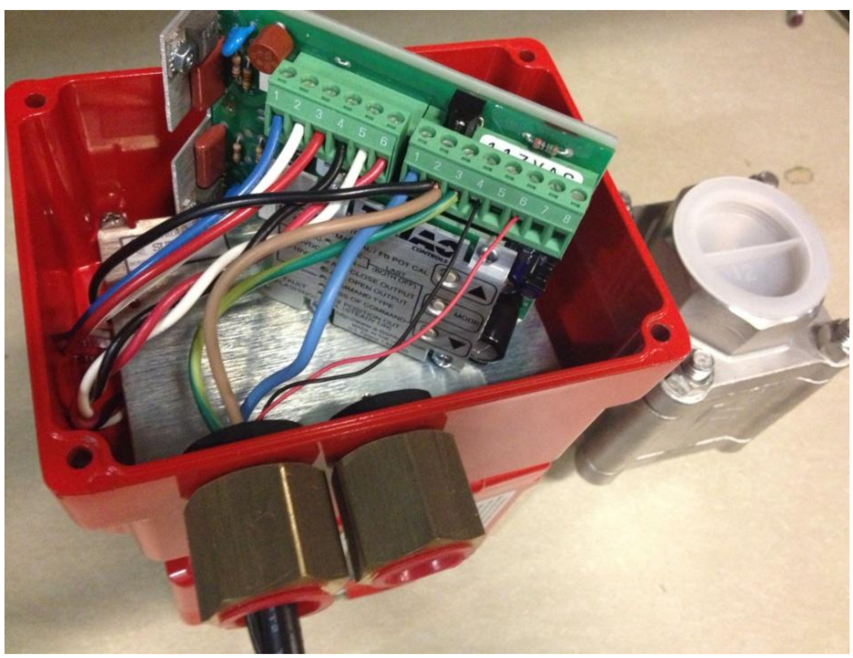

Figure 21 Cable installation for electric valve.

The valve uses a signal of 0-10 VDC and the actuator is powered with 115 VAC. In the documentation that was sent with the valve another part number was found for the servo control, namely DHC-100 instead of TDC-100, according to the manufacturer these have the same specification. Wiring was done according to the instructions found on the 4th page under power/signal.
In the Measurement & Automation Explorer a new virtual channel was created. The physical channel used was Dev2/ao0. And the signal output range was set to 0 to 10 VDC. Terminal configuration was set to reference single-ended voltage signals (RSE) and no scaling was used.

4.6 Camera

In order to check if the valve was operating as expected when it was tried out for the first time a camera was installed above the valve to monitor the open/closing indicator. The valve worked as was expected therefore after a few runs the camera was refitted to monitor the tank and regulator pressure, to make sure the tank pressure did not drop below the regulator pressure while testing was done.

5 LABview

In the wind tunnel lab, labVIEW was used as a measurement and control system (labVIEW version 8.5 updated to versions 2010 and 2011). A National Instruments PCI-6071e was used for data acquisition and to create output signal to the fan, turntable and microjets. Specifications for the PCI-6071e are found in Table 13.

Table 13 Data acquisition properties

Number of channels	**64**
Samples per second	1.25 MS/s
Analog outputs	2
Bidirectional digital channels	8
24 bit counters	2

During my internship in the period after ordering the hardware that was needed I familiarized myself with labVIEW through studying labVIEW Basics 1, 2 and the Data Acquisition and Signal Conditioning Course Manual. When I finished reading labVIEW basics 2 I started building a simple controller for the electronic valve. This would be sufficient for static testing. But for open loop and closed loop testing a more intelligent system would be needed. Therefore I looked into several options. For the microtab control a VI was build for open loop control. In this VI a timed loop is triggered when a gust was started, one by one deploying the tabs. But as the jets behave in a continuous manor in contrary to the tab system, a PID controller would be easier to setup. In a later stadium of my internship I also looked into this. In theory this should also work for closed loop control. The files are either found in my personal folder on the wind tunnel PC (C:\Users\Xander\Documents\Microjet control\) or in the main window folder where basically all other VI's are found that are used.

5.1 Simple valve control (microjet.vi)

The simple controller for the electric valve using continuous single point generation is displayed in Figure 22. This way the output signal will be updated continually.

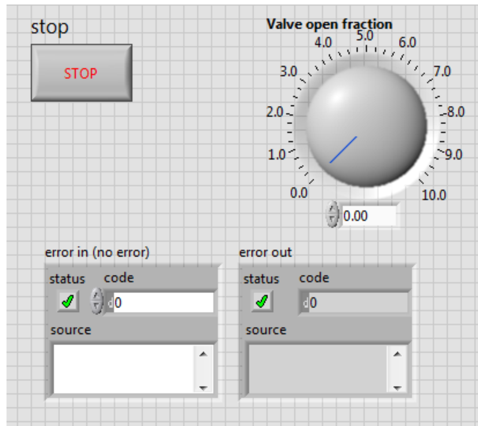

Figure 22 Control panel of the simple valve control.

The front panel consists out of a rotary control to set the valve opening fraction, a stop button and an error indicator. When the rotary control is set to 0 volt the valve will close and it will fully open if it is set to 10 volt. The valve automatically closes when it is powered off.

The block diagram is shown in Figure 23 on the right side. The type of signal that is used is selected at the DAQmx create channel VI, in this case we are creating an analog output, a voltage. This voltage will be supplied to channel ao0 on device 2. The DAQmx start task VI starts the task and because we want the model to continuously supply the voltage the DAQmx write VI is put inside a while loop. The analog double 1 channel 1 sample write task writes a floating point sample to a task that contains a single analog output channel. The connections and icon are shown on the left in Figure 23, the upper left connection is for the physical channels, the one below is for the valve open fraction, the third one is for the stop button, the lower left one is for the error in cluster and finally the lower right one is for the error out cluster.

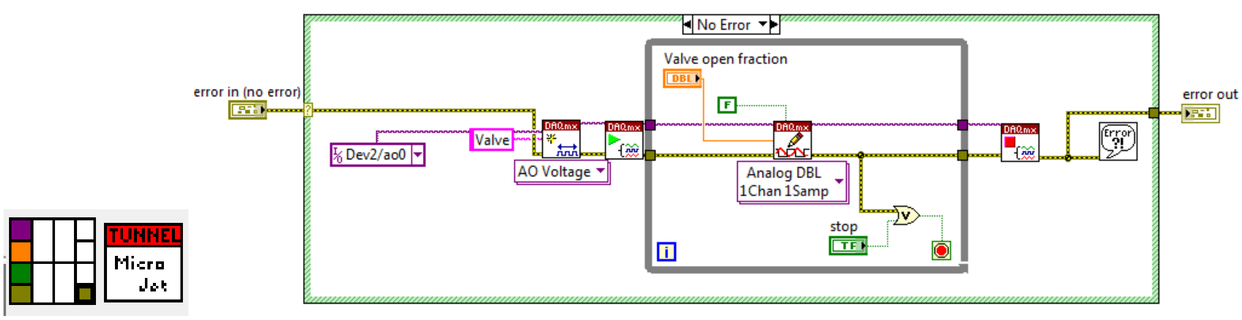

Figure 23 Microjet connection scheme (on the left) and Block diagram of the simple valve control (on the right).

5.2 Implementation simple valve control in Gust VI (Run Gust sim.vi)

For the open loop testing that was done for the tabs a VI was build that would release the tabs when a gust would be incoming. Gradually the tabs would be released one by one, steadily counteracting the change in lift that was caused by the gust. By interchanging the tabs VI with the simple micro jet VI the jets would be triggered counter acting the change in lift at a constant rate, the flow speed of the micro-jets is preset in the simple valve control.

Some changes were made in the Run Gust VI because certain aspects were not needed in the microjet system, the original VI and control panel are found in Figure 40. The direction channels and rate are no longer used because the direction function is not used in the microjet setup at this moment. The signal is constant hence no rate input is needed. The control panel of the microjet sub VI is implemented in the front panel using a new cluster called Valve control. All the controls of the micro-jet sub VI are found there.

5.3 Proportional gain signal-control (PID Control-Signal Source While Loop.vi)

For closed loop control a PID controller is an interesting option, a good point to start is a proportional control. There are a lot of packages available for labVIEW, such as a PID control package. However it is relatively expansive and because the concept is rather simple it was more appealing to build a PID controller VI.

On the National Instrument site an example of an Proportional control is given. A timed loop in conjunction with the signal from tasks DAQmx Timing source is used to setup an analog proportional application. The block diagram of the proportional gain signal-controlcan be seen in Appendix B Figure 39 on the right.The steps describing the process given by National instrument are as follows:

1. Create an analog input voltage channel. Also, create an analog output voltage channel.
2. Set the rate for the sample clock of the analog input and the analog output tasks. Additionally, define the sample mode to be hardware timed single point for both tasks.
3. Call the Get Terminal Name with Device Prefix. This will take a Task and a terminal and create a properly formatted device + terminal name to use as the source of the sample clock for the AO task. By sharing the sample clocks the tasks will be synchronized.
4. Call the Start VI to arm the AO task
5. Use the DAQmx Create Timing Source VI to create a timing source using the AI task. Make sure the analog output task is started before you create the timing task. Wire the timing source out terminal of the Create Timing Source VI to the source terminal of the timed loop.
6. Read the data.
7. Call the Proportional Gain VI. This takes specified set point and gain and calculates the output value given the process variable.
8. Note: For better accuracy the LabVIEW Real Time Toolset provides an optimized PID VI.
9. Write the data
10. Use the Finished Late [i-1] terminal of the Timed Loop to determine if the loop is keeping up.
11. Note: If you are using this VI with LabVIEW Real Time, normally controls and indicators should not be placed inside the time-critical loop. However, for the purpose of instruction and

simplicity, a few controls and indicators are used in this example. Before deploying such an example, the controls and indicators should be replaced by RT FIFO VIs, and data should be communicated to the Host PC through a separate normal priority VI running in parallel to the time-critical application.

12. Call the Clear VI to Clear the Tasks
13. Use the popup dialog box to display an error if any.

Some simplifications were made to the model. There is no need of a timed loop, therefore a while loop is used instead. This also eliminates the DAQmx create timing source. And because the valve needs a single channel single sample signal the DAQmx Read and Write settings were also changed, resulting in the block diagram in Appendix B Figure 39 on the right.

5.4 PID Control (simplepid.vi)

On the LABview website the controller that is seen in Figure 24 was described as a PID controller however it really is just a proportional control. The working principle of a proportional-integral-derivative controller (PID Controller) is showed in Figure 24. The plant or process can be referred to as the airfoil with micro-jet installation. Here y(t), the process output is the measured lift variable, and the setpoint r(t) is the lift that should be generated. The difference between the process variable and the setpoint is the error e(t). Now in the Proportional action, e(t) is multiplied by a constant factor Kp, in the Integral action e(t) is integrated over time and multiplied with a constant factor Ki and the derivative action is found by differentiating e(t) with time and multiplying it with a constant factor Kd. Add all these up, resulting in the controller output u(t) and for this particular case this would be used as the valve input signal.

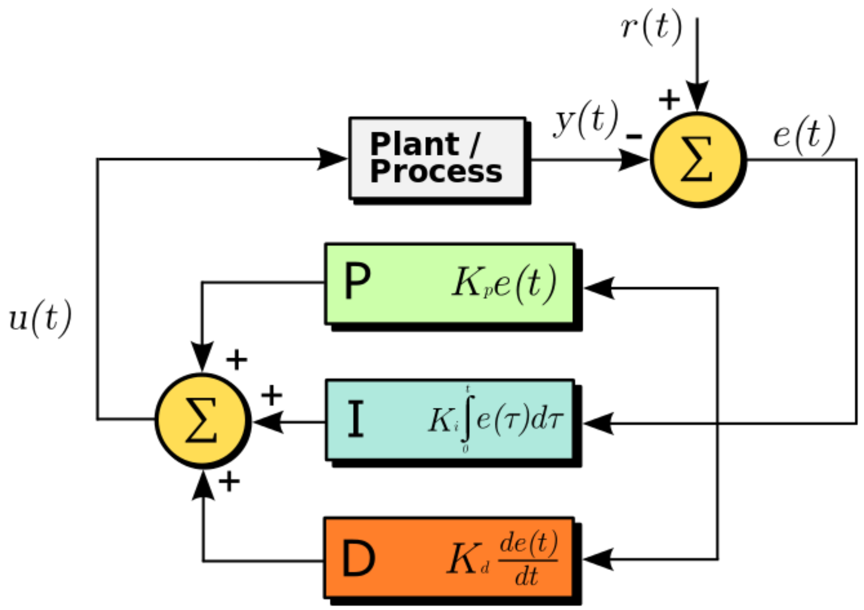

Figure 24 Schematic representation of a PID controller.

On the website of labVIEW there was also a VI of a free PID controller, this is seen in Figure 25. This is just a basic layout that can be used. The PID controller was not implemented on the microjet system because first a correlation between the momentum coefficient C_μ and ΔC_l needed to be found with static testing before the PID controller could be used. In the block diagram a Tick Count is used, in combination with a MathScript so a time based set of algebraic equations can be created. First the error(err) is calculated by subtracting the process variable(pv) from the setpoint (sp). Summing the new error with the old one creates the integrated error(errsum) from time 0 to time t. Every iteration or time step the error is put in the shift register and is used in the next iteration to determine the gradient of the error, the same is done for the time, by dividing the error gradient by the time gradient the derivative of the error to time t is calculated. Now the Proportional (P) term is found when the error *e(t)* is multiplied with a constant *Kp*. The Integral term (I) is found by multiplying the summed error with a constant *Ki.* And the Derivative term (D) is found when the derivative of the error to time is multiplied with *Kd*. Summing P, I and D results in the output of the PID Controller, in Figure 41 in Appendix B. *Kp, Ki* and *Kd* are to be found by trial and error.

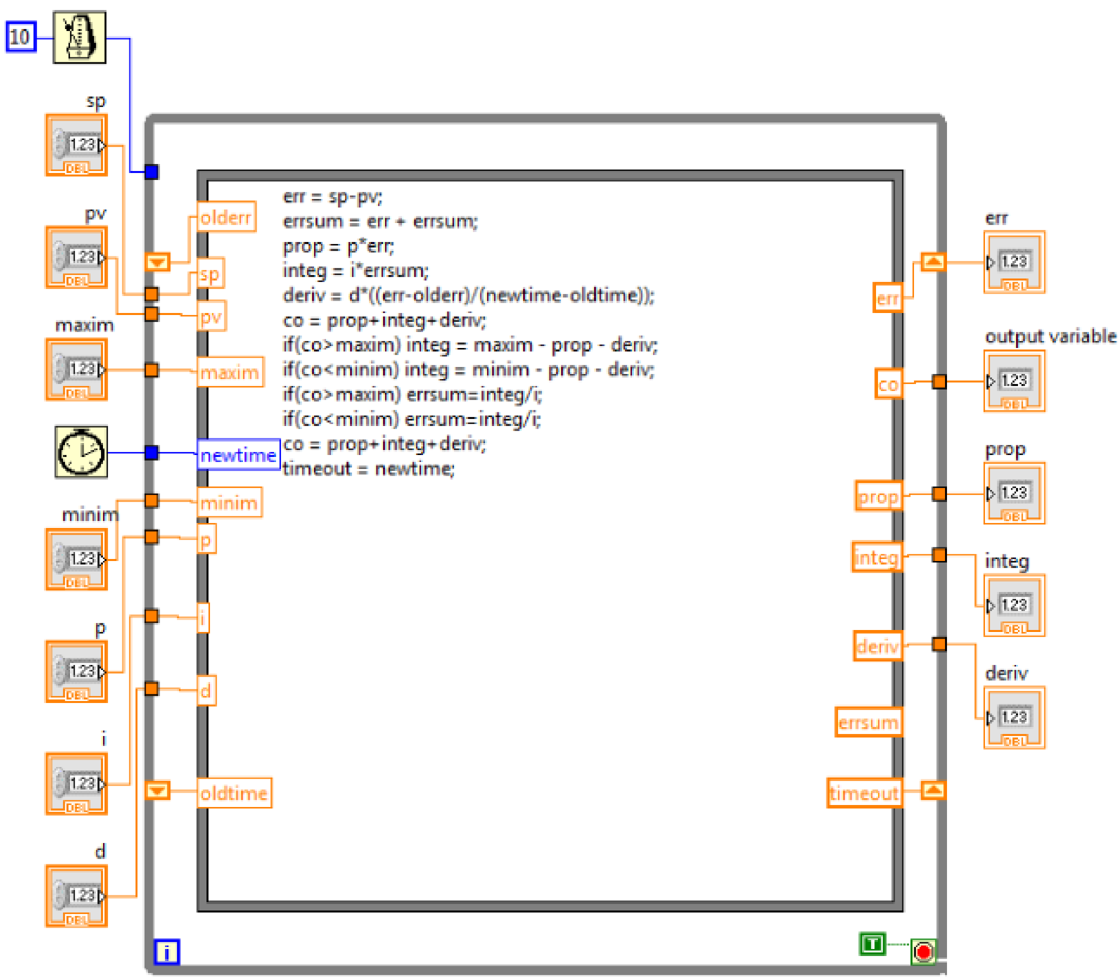

Figure 25 PID controller (www.ni.com)

6 Results

In this section the results of the experiments performed will be described, as are the methods used for testing. First a reference angle sweep is done, repeated two times to test for reproducibility. When the reference is set a series of tests were done to see what the influence of the jets are for various angles of attack and values of C_μ on the lift in time. This type of testing will be referred to as 22.5 seconds monitored tests for microjet influence. Finally an angle sweep was done with either the microjets deployed on the pressure or the suction side.

6.1 Labview results

In the existing labVIEW VI used to operate the wind tunnel there was a program already written to output all the properties measured by the different sensors used. The sensors output a voltage which is translated to SI or in Imperial units by multiplying with a certain conversion factor, which was already programmed. The balance measures the lift (lb), drag (lb), side force (lb) pitching moment (ft-lb), yaw (ft-lb), roll moment (ft-lb), φ (deg), α (deg) and θ (deg). Because we are looking at a two dimensional model the lift for our model is the side force and the angle of attack is φ, but in when the angle of attack is referred to in the report, α will be used. Besides this there are sensors for the atmospheric pressure (PSI) and the atmospheric temperature (C°).

The properties of an airfoil are often translated into dimensionless properties such as C_l, C_d and C_m:

$$C_l = \frac{L}{\frac{1}{2}\rho v^2 S}, C_d = \frac{D}{\frac{1}{2}\rho v^2 S}, C_m = \frac{M}{\frac{1}{2}\rho v^2 Sc}$$

All the parameters in these formulas are evaluated in SI units. In these formulas L indicates Lift (N) (side force in the results from lavVIEW), D indicates drag (N), M the pitching moment (Nm), v the air speed (m/s), S the platform area (m^2) and c the chord of the airfoil (m). However the density of the air is not measured and needs to be determined using the perfect gas law:

$$P = \rho RT \rightarrow \rho = \frac{P}{RT}$$

The results from labVIEW are given in imperial units. Therefore to determine Cl, the lift, air density and air speed were converted into SI units.

6.1.1 Data acquisition

Sampling was done at 3000 Hz and averaged over 2 seconds. Every 500 samples are averaged, resulting in an effective acquisition rate of 3 Hz, resulting in 6 values for every acquisition point. For readability the average of these 6 measurements is plotted for each data point.

6.1.2 Calibration and test preperation

Before testing, labVIEW needs to be configured. The channels that need to be monitored are selected, the latest calibration files are loaded, the airfoil type is selected (the modified S819 model in this case), the chord and the respective area ($\text{span} \times \text{chord}$) and finally it needs to be specified not to use the Interaction Card. After the calibration in labVIEW is done all the forces on the balance monitor are set to zero, this was repeated every time the wind tunnel was turned off and on. Before every test the space in front of the wind tunnel was swept clean and it was made sure that there were no lose obstacles in front of the wind tunnel.

6.1.3 Momentum Coeficient C_μ

In many of the results following the momentum coefficient, C_μ, is used to describe the momentum delivered by the jets. The momentum coefficient relates the momentum of the fluid to that in the free steam according to:

$$C_\mu = \frac{\dot{m}_{jet} U_{jet}}{q_\infty bc} = 2\left(\frac{b_{jet}}{b}\right)\left(\frac{c_{jet}}{c}\right)\left(\frac{U_{jet}}{U_\infty}\right)^2$$

In the above formula b_{jet} and c_{jet} represent the width and length of the jet exterior machined in the airfoil, U_{jet} and $\dot{m}_{jet}$ are the air speed and mass flow of the jet. The parameters *b* and *c* represent the airfoil span and chord of the airfoil, q_∞ and $U_\infty$are the dynamic pressure and flowspeed of the free stream in the wind tunnel.

The data from the wind tunnel measurements did not give C_μ directly. In a Matlab file the collected data was used to calculate C_μ. The unity of the airspeed that was specified in the labVIEW spreadsheet was not given; therefore this was checked with Sutherlands law. With Sutherland's law it is easy to calculate the free stream air speed from the Reynolds number. In the figures that use C_μ the calculated air speed was used instead of the one from the wind tunnel data. Because the Reynolds number is calculated from the airspeed this should give about the same answer because the temperature from the collected data was used in the calculation.

6.2 Reference testing

As a reference for the modified S819 model, of which the dimensions are given in Table 5, before testing the jets an angle sweep was done with the jets turned off. This test was done 3 times to check the reproducibility. The angle sweep was performed at $Re = 500 \times 10^3$, an atmospheric pressure of approximately 101.2 kPa, an atmospheric temperature of approximately 298 K. The result of this can be seen in Figure 26. The results confirm that the airfoil is not symmetrical because Cl is not zero at zero angle of attack. Stall occurs gradually around 13 degrees where the highest Cl is found at a value of about 1. These are expected results for such an airfoil, hence the calibration was done well and therefore the results can be studied further.

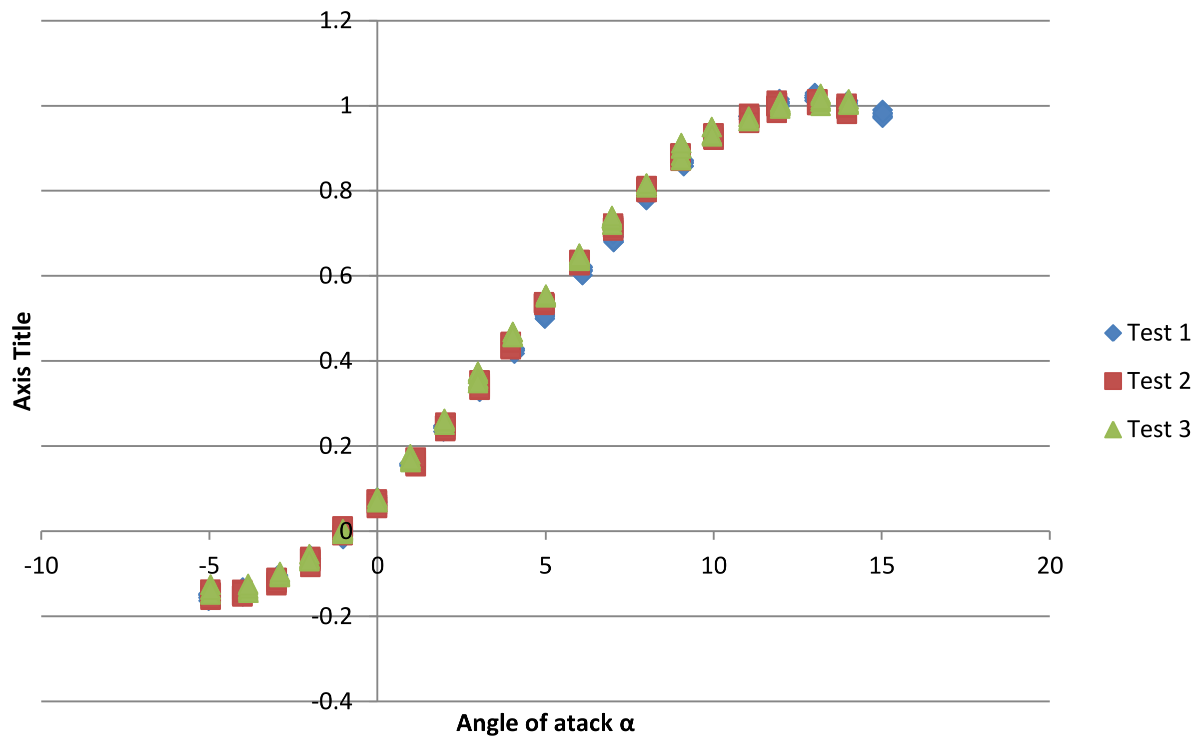

Figure 26 Refernce test done 3 times for reproducibility concerns.

6.2.1 Static testing dcl/dα

According to Prandtl in his thin airfoil theory the slope of the lift coefficient should be 2π per radiant which is equal to 0.11 per degree. In this case using the modified S819 airfoil dcl/dα = 0.9. The deviation is caused by 3D properties of the airfoil, it is not infinitely long.
The slope was measured between 0 and 8 degree angle of attack, at higher angle of attack stall starts to occur.

6.3 22.5 seconds monitored tests for Microjet influence

6.3.1 Testing protocol

The tunnel is run at wind speeds that result in a Reynolds number of 500,000. For angles of attack 0, 4, 8 and 12 degrees, with the jets on the pressure side hooked up to 15 PSI pressurized air. For each angle four different flow rates were tried out, the valve was stroked to 20%, 40% and 60%. In the rest of the section those will be referred to as case 1 with low flow rate (±20 SCFM), case 2 with moderate flow rate (±70 SCFM) and case 3 with high flow rate (±110 SCFM) in ascending order.
For all three cases, at the above mentioned angles of attack, measurements were taken for 22.5 seconds. Before the measurements were started the angle of attack was set and the free stream velocity was increased until the reference Reynolds number was met. Aspects of interest are the flow rate against the time and the lift against the time. The data acquisitioning was done the same way as the reference case was done.

6.3.2 Results

The characteristics for the different microjet flow rates showed to be very similar, therefore only one of the cases is showed in this section. In case 2 with moderate flow rate the results are better noticeable than in case 1 with low flow rate. And in case 3 there was a hiccup causing the valve to open slightly later with α = o degrees, making the results less accurate. Plots of case 1 and case 3 are found in Appendix B.

Figure 28 shows the change in C_l caused by the jets in time. Figure 27 shows the flow speed of the jets changing in time. In each figure there are four different data series shown for 0, 4, 8 and 12 degrees angle of attack. At the start of the test the valve is closed and is gradually stroked up to 20%, 40% or 60%. When the valve is stroked up to 40% the microjet flow rate is approximately 71 SCFM ($C_{\mu,avg} = 2.06 \times 10^{-3}$), when the valve is stroked to 20% the microjets acquire a flow rate of about 19 SCFM ($C_{\mu,avg} = 1.42 \times 10^{-4}$) and when it was stroked to 60% the microjet flow rate is about 115 SCFM ($C_{\mu,avg} = 5.59 \times 10^{-3}$).

In Table 14 the average (μ), standard deviance (σ) and the variance (σ2) of C_l is given all three cases. The data was determined using the average, stdeva and var function of Microsoft Excel 2007. Besides this the decrease in Cl (ΔC_l) is given for each case. At start of the measurements for 4 seconds the microjets were not used, in Table 14 the measurements that were taken in this time frame are referred to as "Reference". After 4 seconds into the measurements the microjets are turned on, the valve is stroked up to 20%, 40% or 60% of full stroke. Then after the flow conditions have stabilized the microjet induced data is gathered, depending on the case this was 11 seconds after the first measurement when the valve was stroked to 20%, 12 seconds when the valve was stroked up to 40% or 14 seconds when the valve was stroked up to 60%. In

Table 14 this is referred to as "With microjets".

For all three cases ΔC_l remains almost equal when the α is ramped up from 0 to 12 degrees angle of attack. For the 40% stroke data series, ΔC_l at $\alpha = 0$ is 0.107, compared to 0.124 for $\alpha = 4$ and 0.113 at $\alpha = 8$. The differences in ΔC_l for the varying angles of attack stay well within the standard deviation range ($\Delta Cl_{4^\circ} - \Delta Cl_{0^\circ} = 0.017$, $\sigma_{0^\circ} = 0.019$). Thus it can be concluded that the difference is caused by the signal noise. For $\alpha = 12$ ΔC_l is only 0.055, which is about half of the ΔC_l measured at $\alpha = 0$, $\alpha = 4$ and $\alpha = 8$. The same behavior is seen in case 1 and case 3, the low and high flow rate cases, and can be explained due to stall effects.

Table 14 Statistic results from 22.5 second jet startup tests. "Reference" time frame with jets off (t< 4 seconds after startup). "Microjets" time frame with jets on after flow is stabilized (t > 8 seconds after start up depending on how far valve is stroked).

	μ_{Cl} Valve Stroked 20% ($\times 10^{-1}$)	σ_{Cl} Valve stroked 20% ($\times 10^{-2}$)	σ^2_{Cl} Valve stroked 20% ($\times 10^{-4}$)	μ_{Cl} Valve Stroked 40% ($\times 10^{-1}$)	σ_{Cl} Valve stroked 40% ($\times 10^{-2}$)	σ^2_{Cl} Valve stroked 40% ($\times 10^{-4}$)	μ_{Cl} Valve Stroked 60% ($\times 10^{-1}$)	σ_{Cl} Valve stroked 60% ($\times 10^{-2}$)	σ^2_{Cl} Valve stroked 60% ($\times 10^{-4}$)
Reference α=0	0.834	1.77	3.12	0.871	1.89	3.59	0.856	1.72	2.95
Microjets α=0	0.572	1.79	3.19	0.195	2.50	6.26	1.23	2.43	5.92
Reference α=4	4.18	2.28	5.21	4.25	1.73	3.01	4.33	1.89	3.58
Microjets	3.94	1.74	3.04	3.02	1.86	3.44	1.91	2.06	4.25

α=4									
Reference α=8	7.69	2.10	4.40	7.69	2.07	4.27	7.74	2.18	4.77
Microjets α=8	7.39	1.94	3.77	6.56	1.95	3.82	5.52	2.08	4.31
Reference α=12	7.90	3.15	9.92	7.97	2.95	8.68	7.95	2.52	6.36
Microjets α=12	7.79	2.52	6.34	7.41	2.78	7.72	6.80	2.88	8.31

Table 15 Average difference between the reference C_l and stroked valve C_l.

$\Delta\mu_{Cl}$	Valve stroked 20% $(\times 10^{-2})$	Valve stroked 40% $(\times 10^{-1})$	Valve stroked 60% $(\times 10^{-1})$
α=0	2.62	1.07	0.208
α=4	2.47	1.24	2.42
α=8	2.98	1.13	2.22
α=12	1.10	0.053	1.14

There were also some unexpected results, the flow speed increased overtime after the flow stabilized for all flow cases. This can be seen very clearly for case 2 (moderate flow) in Figure 27, but the same characteristic is also seen for case 1 and case 3 in Figure 35 and Figure 37 in Appendix B. It is important to know how much of an effect this has on C_l when compared to the increase in flow rate. In Table 16 and Table 17 the flow speed and C_l increase is give, besides this the percentage of the mean measured flow rate and C_l is given. As can be seen the influence is minimal, because the time interval of the experiment is small, a few percent at the most.

Table 16 Percentage microjet flow rate increase compared to mean, measured over time after flow conditions have stabilized with the valve stroke and angle of attack kept constant.

Angle of attack	Flow rate increase (%), stroke 20%	Flow rate increase (%), stroke 40%	Flow rate increase (%), stroke 60%
α=0	0.368	1.78	1.56
α=4	0.921	1.27	1.97
α=8	0.929	1.26	1.81
α=12	0.739	1.47	1.56

Table 17 Percentage Cl change compared to mean, measured over time after flow conditions have stabilized with the valve stroke and angle of attack kept constant.

Angle of attack	Cl change (%), stroke 20%	Cl change (%), stroke 40%	Cl change (%), stroke 60%
0	4.29	0.64	2.35
4	0.64	0.52	3.89
8	0.16	1.30	1.68
12	0.02	1.25	0.92

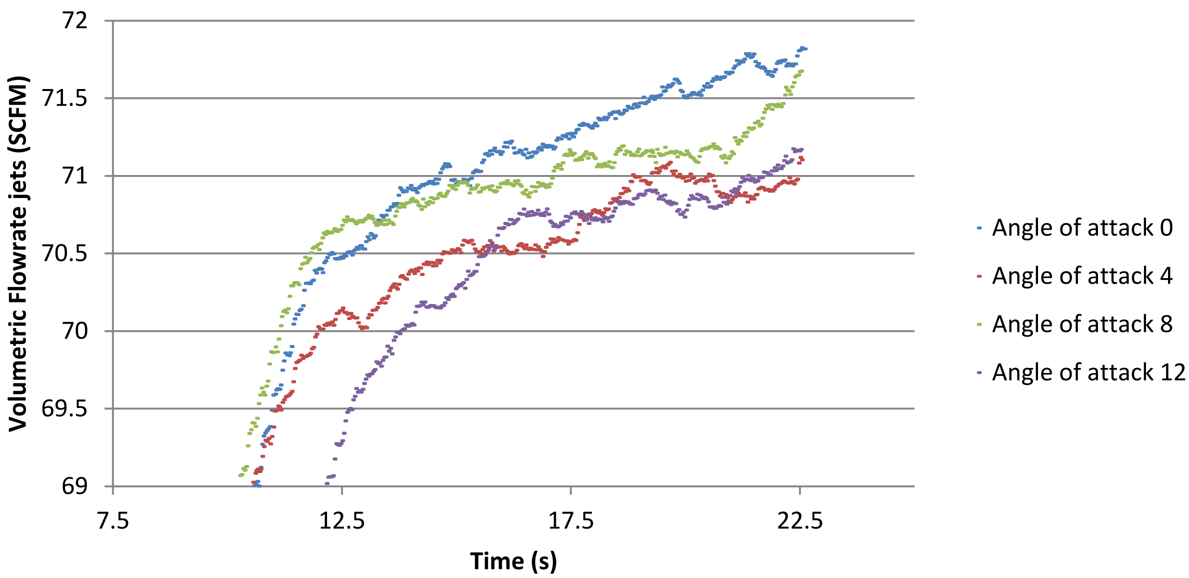

Figure 27 Volumetric flow rate (SCFM) response for 40% valve stroke.

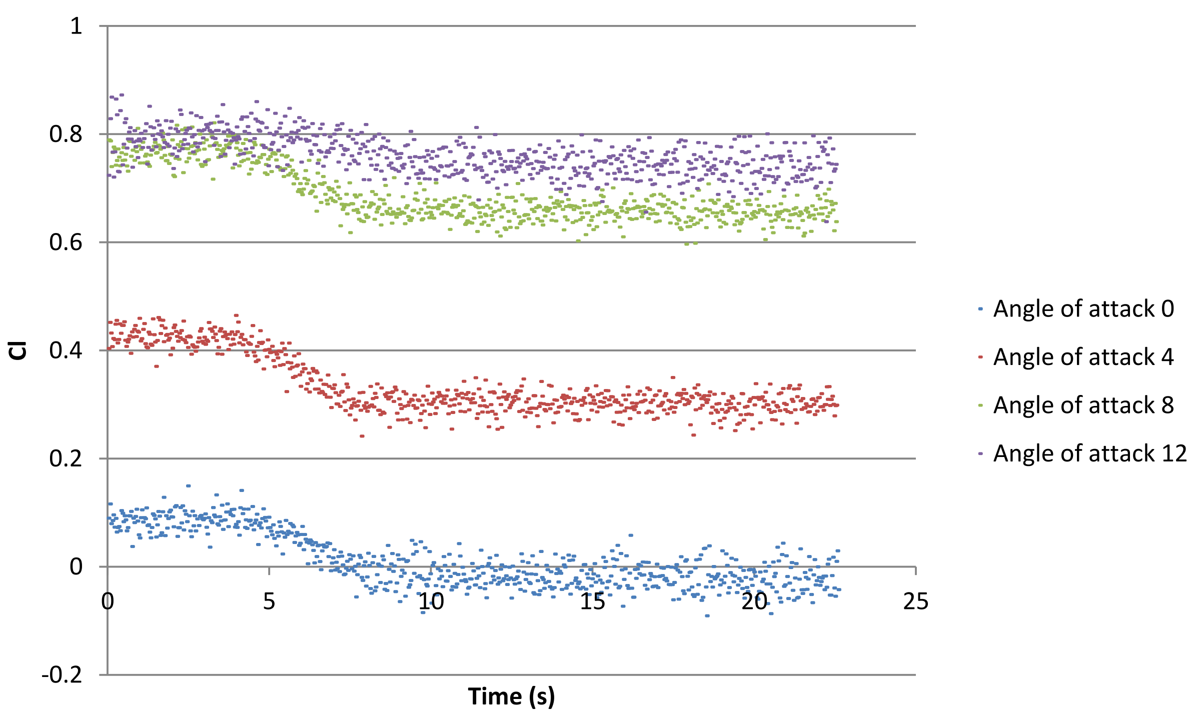

Figure 28 Cl response when jets are turned on up to 40% valve stroke.

7 Angle sweep

In this section the results of an angle sweep with the microjets is described. We are only interested in lift. Drag and the momentum coefficient are not studied.

7.1 Testing protocol

An angle sweep is performed ranging from a -4 to 14 degree angle of attack in steps of 2 degree. Again three different microjet flow rates were used. In Case 1 with low flow rate the valve is stroked to 20% (±20 SCFM, C_{μ} = 0.0001), in case 2 with moderate microjet flowrate the valve was stroked to 40% (±70 SCFM, C_{μ} = 0.0021) and in case 3 with high flow rate the valve was stroked to 60% (±115 SCFM, C_{μ} = 0.0050). The supply pressure was set to 14 PSI for the suction side jets and to 15 PSI for the pressure side jets. After the suction side jets angle sweep was performed and the air supply fitted to the suction side jets first the turntable was recalibrated.

For both angle sweeps the Reynolds number was kept constant at 500.000 throughout the angle sweep. For case 1 and case 2 one full tank of air at 80 PSI was enough to supply the jets throughout the angle sweep. In the 3rd case the tank emptied much quicker. For a total angle sweep 3 full tanks at 80 PSI were emptied. At first the wind tunnel was turned off when it was filled up while it took about 20 minutes to fill the tank up to 80 PSI. The results that came out where qualitative of worse condition than the 20% and 40% stroke test. Looking closer at the results it appeared that the flow rate increases with time just after the valve is opened. First it was tried to use steps of 3 degrees angle of attack to minimize the number of points measured to reduce testing time, however even then one full tank did not contain enough air to do a full angle sweep. Later on with the testing of pressure side jets again steps of 2 degrees angle of attack were used.

The reference used is the data from test 1 in Figure 26, due to a very limited time for testing no second reference was made after the air supply was refitted to the pressure side jets. However the turn table was recalibrated and all the forces and moments where set to 0.

7.2 Data verification

The data acquired in the angle sweep for the suction side jets should be the same for similar operational conditions (angle of attack and valve stroke) to the data acquired in the 22.5 seconds startup tests after the jet velocity has stabilized. In Table 18, Table 19 and Table 20 the Cl data from the 22.5 seconds startup test is compared to the angle sweep data, for all the valve setting the 22.5 seconds startup test is significantly higher.

Reassessment of the data shows there was an offset of about +2 degree in the turntable calibration for the suction side angle sweep. By comparing and linear interpolation of the data the offset in the angle of attack in the suction side angle sweep test was calculated, this was done for all 3 cases for $\alpha = 0$, $\alpha = 4$ and $\alpha = 8$. Results of this analysis are seen in Table 21.

Table 18 Cl comparison Angle sweep and 22.5s startup test for case 1 (20% stroke,±20 SCFM).

α	Measured C_l angle sweep ($\times 10^{-1}$)	Measured C_l 22.5s startup test ($\times 10^{-1}$)
0	-0.94	0.57
4	1.99	3.94
8	5.30	7.39
12	7.29	7.79

Table 19 Cl comparison Angle sweep and 22.5s startup test for case 2 (40% stroke,±70 SCFM).

α	Measured C_l angle sweep ($\times 10^{-1}$)	Measured C_l 22.5s startup test ($\times 10^{-1}$)
0	-1.55	-0.20
4	1.32	3.02
8	4.53	6.56
12	6.98	7.41

Table 20 Cl comparison Angle sweep and 22.5s startup test for case 3 (60% stroke,±115 SCFM).

α	Measured C_l angle sweep ($\times 10^{-1}$)	Measured C_l 22.5s startup test ($\times 10^{-1}$)
0	-3.14	-1.23
4	-0.47	1.91
8	2.72	5.52
12	5.88	6.80

Table 21 Angle of attack offset for the 0, 4 and 8 degree angle of attack for 20, 40 and 60% valve stroke usage.

Angle of attack α (˚)	Offset for 20% stroke (˚)	Offset for 40% stroke (˚)	Offset for 60% stroke (˚)
0	2.07	2.06	1.85
4	2.14	2.13	2.17
8	1.95	1.89	2.04

7.3 Data correction

Now it is clear that there is an offset for the measured angle of attack in the acquired data a plan has to be determined. Best would be to recalibrate the tunnel and repeat the experiment, however this clearly is not an option at the moment in time, therefore the offset will be corrected using the average values for case 1,2 and 3, given in Table 22. Therefore all the following graphs for the suction side jets angle sweep will be the corrected data.

Table 22 Average measured offset for 20, 40 and 60% stroke jet usage.

Average offset 20% stroke (˚)	Average offset 40% stroke (˚)	Average offset 60% stroke (˚)
2.05	2.03	2.02

7.4 Suction side Cl-α curve

In Figure 29 an angle sweep is shown for 5 different data series. The first 4 cases are as explained in testing protocol, the fifth data series is comparable to case 3 with high flow rate (±115 SCFM, C_μ = 0.005) only here steps of 3 degrees angle of attack were taken, this will be referred to as case 4.
Another thing that is prominent in the data is the fact that for the 40% stroke case as the 60% stroke case show no clear stall point. In earlier research done with almost the same setup this behavior was described as being interference of the tubing on the balance (Cooperman, 2012).

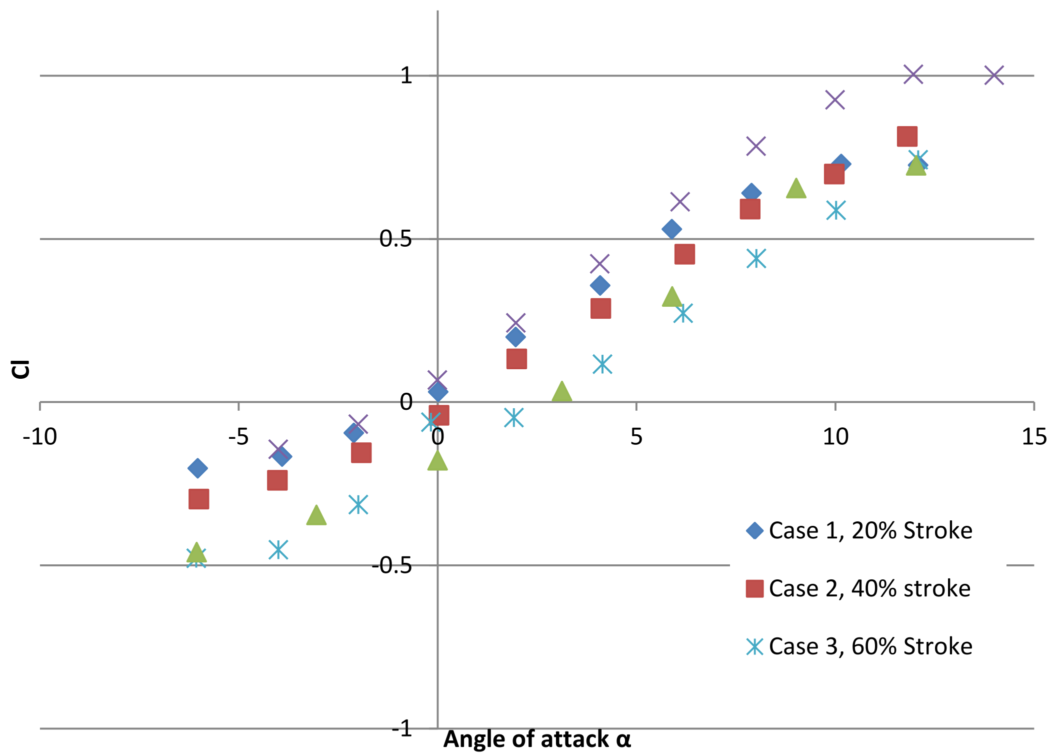

Figure 29 Cl-α curve for Re = 500.000 with the suction side jets used, supplied with 14 PSI air.

7.5 Pressure side Cl-α curve

In Figure 30 the Cl-α curve for the pressure side microjets is seen. Here 4 different data series are seen, as is explained in the testing protocol. For case 2 the 14 degree data point was not used because the supply pressure from the tank was too low. For case 3 again the tank was refilled 2 times. For this reason the results of case 3 are not as smooth as for case 1 and 2. As was discussed in 6.3.2 it takes 7 seconds for the flow to stabilize for case 3 and there is just enough air in the tank to supply the microjets for 20 seconds. The main reason for this is that the cycle time of the electric actuator is between 12 and 14 seconds. In case 3 the valve is opened up to 60% stroke, hence it takes more than 6 seconds to stroke the valve for 60%. This makes it very hard to get qualitative data. In practice it proves hard to tell whether the flow has stabilized properly. In some measurements the flow did not stabilize properly which resulted in a shift in C_l for subsequent measurements.

The influence of the pressure side microjets is less dominant than with the suction side microjets. The lift coefficient is lower in case 1 and 2 compared to the reference case with no jets used. This could be caused by disturbance of the laminar flow resulting in lower lift.

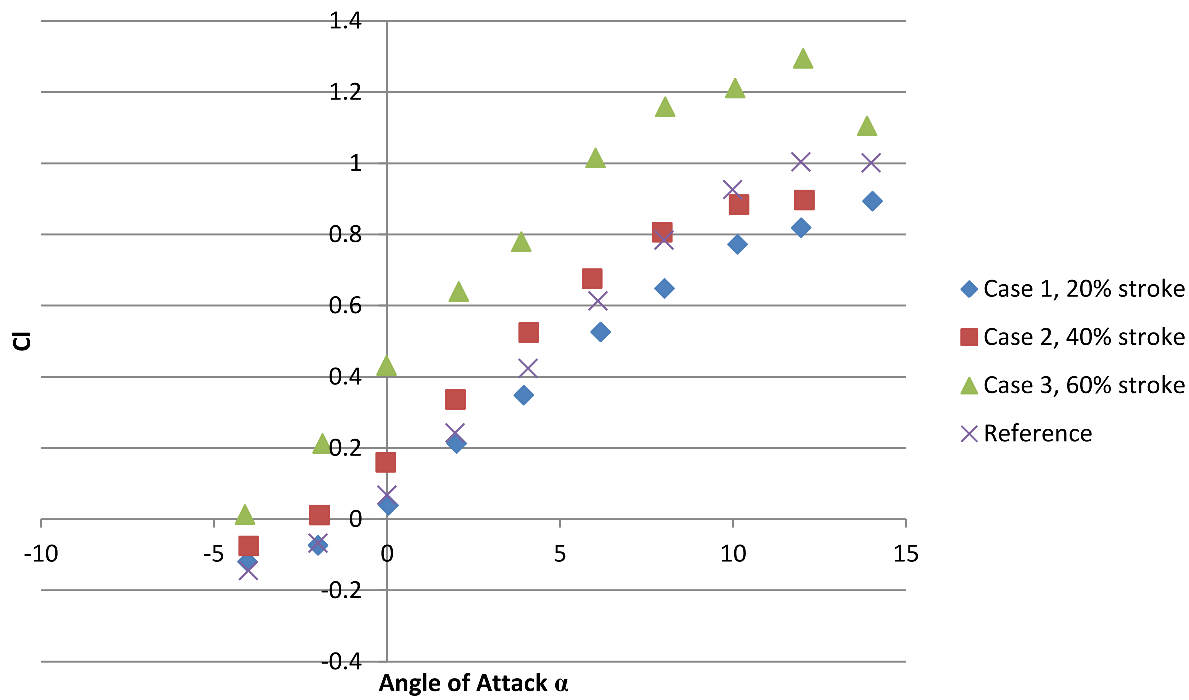

Figure 30Cl-α curve for Re = 500.000 with the pressure side jets used, supplied with 15 PSI air.

7.6 Angle sweep $dC_l/d\alpha$ slope

When the microjets are applied with a constant Cμ, $dC_l/d\alpha$ should be the same as in the reference case. However with changing angle of attack the pressure over the airfoil changes causing Cμ to increase or decrease very slightly. Because of this $dC_l/d\alpha$ is differs from the reference case, the results are seen in Table 23. For the suction side microjets the slope decreases with about 20% for all microjet flowrates. For the pressure side jets the slope of lift curve $dC_l/d\alpha$ drops and then increases for increasing flow rates. Case 1 has a slightly smaller slope than the reference, for case 2 the slope is almost equal to the reference, and case 3 has a slope that is larger than the reference case.

Table 23 dCl/dα for 20 to 60% valve stroke

Valve opening	Suction side dCl/dα (1/˚)	Pressure side dCl/dα (1/˚)
No jets	0.089	0.089
20% stroke (20 SCFM average)	0.075	0.079
40% stroke (73 SCFM average)	0.072	0.086
60% stroke (115 SCFM average)	0.075	0.096
60% stroke 3 deg. Step (116 SCFM average)	0.075	

7.7 Maximum lift coefficient, Cl_{max}

The maximum Cl is found at the same angle of attack for when the suction or pressure side jets are used compared to the reference no jet case. Only case 2 for both the suction and the pressure jet data in Table 24 differ. Table 24 shows a 2 degree increase for when the pressure side jets are used and a 2 degree decrease for the when the suction side jets are used. Which is actually against expectations, because Figure 29 and Figure 30 suggest that the Cl-α curve is shifted to the right when the suction side jets are used and shifted to the left when the pressure side jets are used. This conclusion is drawn because stall occurs later when one studies Figure 29 and Figure 30 for when either the suction or pressure side jets are used. In the research done by (Cooperman, 2012) the same behavior was found, here this was explained by interference that the tubing of the jets have on the balance. Because of this the actual Cl is slightly lower for angles of attack higher than 8 degree.

Table 24 Clmax measured for the suction and pressure side jets used.

Valve opening	Suction side		Pressure side	
	Cl	α (˚)	Cl	α (˚)
No jets	1.02	12.0	1.02	12.0
20% stroke (20 SCFM average)	0.78	10.2	0.93	14.0
40% stroke (73 SCFM average)	0.86	11.8	0.98	12.1
60% stroke (115 SCFM average)	0.77	12.1	1.36	12.0
60% stroke 3 deg. Step (116 SCFM average)	0.77	12.0		

7.8 ΔC_l and C_μ

Earlier the concept of the momentum coefficient was introduced, a parameter that relates the momentum of the jets with the momentum of the free stream. Delta Cl is the difference between the C_l for the reference no jet case and the C_l for the jet case for an angle of attack ranging from -4 to 14 degrees.

Suction side microjets

The formula for Cμ was given in section Momentum Coeficient Cμ , ΔC_l is evaluated by subtracting the C_l value that was measured with the jets used minus the C_l value where no jets are used, showing a direct result of the jets.

$$\Delta C_l = C_{l,jets} - C_{l,ref}$$

In Figure 31 $\Delta C_{l,suction}$ and C_μ are presented for the suction side for varying angle of attack α. Only the data from case 1 and 2 prove to be useful, in case 3 the air tank needed to be filled up 2 times during the angle sweep. The last measurement before refilling the tank(at α = 0) was taken when the pressure in the tank had dropped below the regulator pressure (15 PSI) causing $|\Delta C_l|$ and C_μ to drop suddenly. Because of this discontinuity in the data it was best to look past the data of case 3 and focus on case 1 and 2. Both the case 1 and case 2 give a $\Delta C_{l,suction}$ that could be expressed with a second order Taylor series(found using the trend line function of excel), with x the angle of attack in degrees:

$$\Delta C_{l,\text{suction}}(\text{case } 1) = -1.4 \times 10^{-3}x^2 - 3.9 \times 10^{-3}x - 0.0253$$

$$\Delta C_{l,\text{suction}}(\text{case } 2) = -7.0 \times 10^{-4}x^2 - 5.3 \times 10^{-3}x - 0.1015$$

But it has to be kept in mind that at higher angles of attack, at angles of attack above 6 degree, the jet tubing introduces interference in the balance, resulting in slightly higher ΔC_l values, which is not represented in the formulas above.
From the data of case 1 and 2 it seems there is a linear relation between C_μ and α. It is clear that this the slope is very small, in a range of 16 degrees (-4 to 12 degree angle of attack) there is only an 5.45% for case 1 and 16.59 percent increase for case 2.

$$C_{\mu,\text{suction}}(\text{case } 1) = 5.0 \times 10^{-7}\text{x} + 1.0 \times 10^{-4}$$

$$C_{\mu,\text{suction}}(\text{case } 2) = 2.0 \times 10^{-5}\text{x} + 2.0 \times 10^{-3}$$

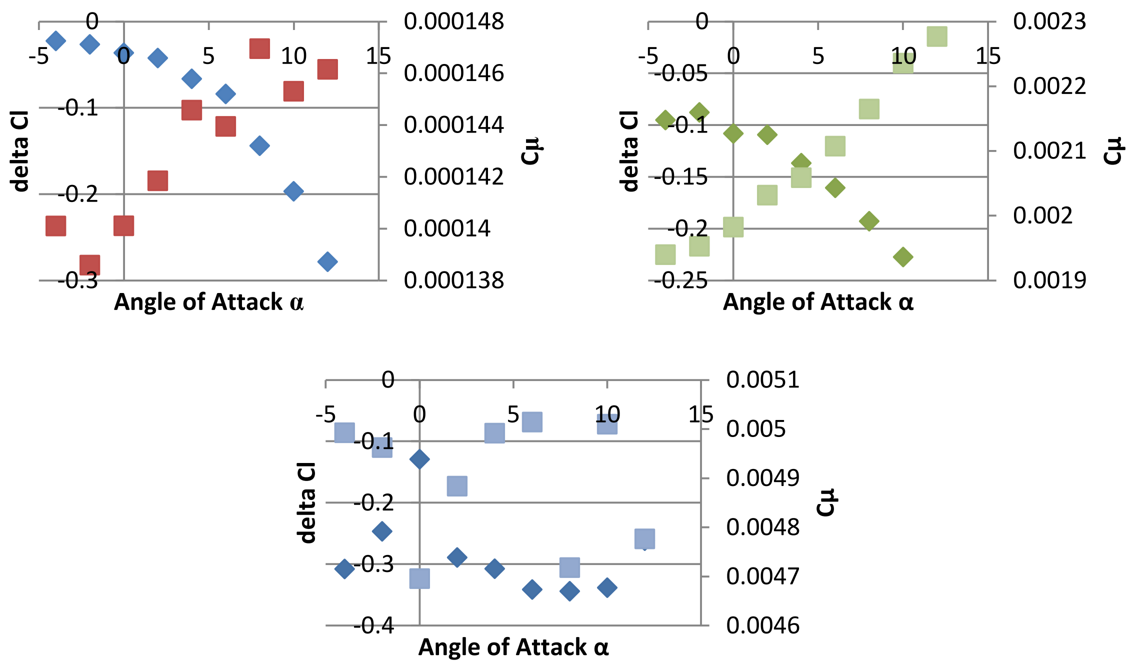

Figure 31 Suction side Delta Cl(diamond) and C_μ(square). Upper left (red and blue) case 1 (20% stroke), upper right(green and orange) case 2 (40% stroke), lower center (light blue and dark blue) case 3 (60% stroke).

7.8.1 Pressure side jets

In Figure 32 ΔC_l and C_μ are plotted against the angle of attack. For case 2 ΔC_l(the orange diamonds in Figure 32) increases slightly for small angles of attack, but for higher angles of attack $\Delta C_{l,\text{pressure}}$ decreases and becomes negative for angles of attack higher than 9˚. The same behavior is, seen in case 3 (dark blue diamonds in Figure 32), for angles of attack higher than 6˚ degrees ΔC_l decreases rapidly. The same problem that occurred with the suction side is recurring here, discontinuity of ΔC_l and C_μ. Therefore again only case 1 and 2 are studied.For case 1 there seems to be a linear relation between α and C_μ and also between α and ΔC_l. For case 2 there is a suitable linear trend line for that fits C_μ as a function of α, for α and $\Delta C_{l,pressure}$ there first is a linear relation but stall occurs at lower angles of attack resulting in a sudden fall in $\Delta C_{l,pressure}$, this can best be described by a 2nd order polynomial.

$$\Delta C_{l,pressure}(\text{case 1}) = -1.0 \times 10^{-2}x - 2.0 \times 10^{-2}$$

$$\Delta C_{l,pressure}(\text{case 2}) = -1.7 \times 10^{-3}x^2 + 3.5 \times 10^{-3}x + 0.1$$

$$C_{\mu,pressure}(\text{case 1}) = 6.0 \times 10^{-7}\text{x} + 1.0 \times 10^{-4}$$

$$C_{\mu,pressure}(\text{case 2}) = 1.0 \times 10^{-5}\text{x} + 2.0 \times 10^{-3}$$

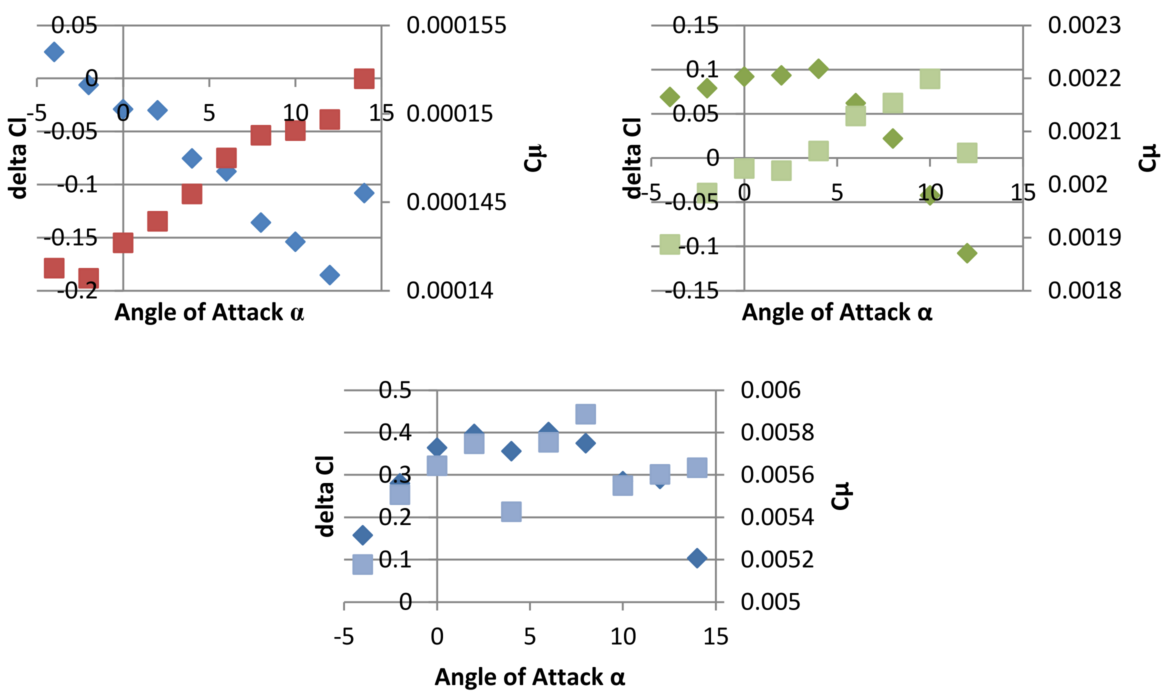

Figure 32 Pressure side Delta Cl(diamond) and C_{μ}(square). Upper left (red and blue) case 1 20% stroke, upper right (green and orange) case 2 (40% stroke) and lower center (light blue and dark blue) case 3 (60% stroke).

7.9 Data verification ΔC_l profile.

Because it is difficult to see a reoccurring profile in the $\Delta \mathbf{C_l}$ plot it is doubtful that the data is correct, especially for the pressure side jet experiments. In Figure 33 the $\Delta \mathbf{C_l}$ profile for various jet flow options is compared to earlier research done on the same model , the results do not match closely. Because of the higher Reynolds number, at which was tested in the earlier research, flow separation occurs later, therefore the results are expected to differ for high angles of attack. Also in the right figure the results were altered to compensate for the interference the tubing has on the balance. But it was not to be expected that the results would differ this much, the trend in the left figure is negative for high angles of attack while for the right figure the trend is positive for high angles of attack.

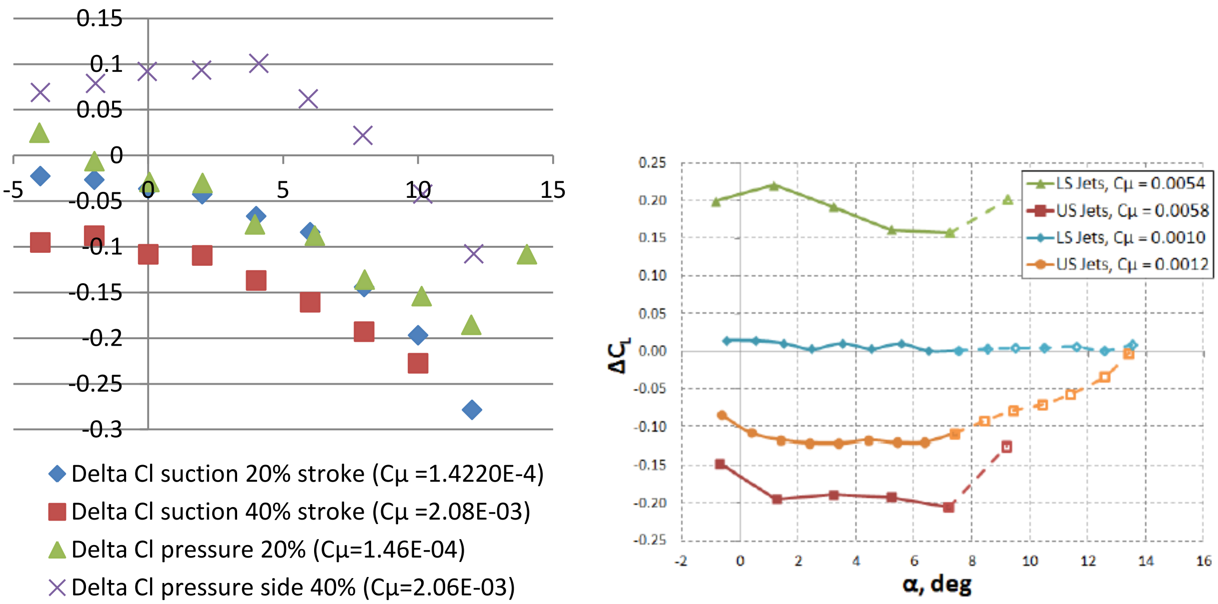

Figure 33 Left ΔC_l for suction and pressure side jets ($Re = 5.0 \times 10^5$) for the new setup and right the results from earlier research ($Re = 1.0 \times 10^6$) (Cooperman, 2012)

8 Costs

In this section the costs that were made on the microjets system while I was doing my internship at UC Davis are shown. This involves the equipment that was bought and also the cost made for installment of the air tank and the plumbing of the tank. In Table 25 an overview of the equipment bought is given with description and pricing.

Table 25 Pricing on equipment bought and installed during my Internship.

Date	Manufacturer / Service Provider	Description	Cost ex. tax	Cost inc. tax
4/16/2013	Applied Valves and Controls	11/2" NPT V Series Control Valve, carbon steel body, 316 stainless steel ball & stem STFE seats, 30 degree v-port ball, mounted with WED-500 high resolution modulating electric actuator, 115VAC power supply, with TDC-100 servo card, 0-10VDC command signal	$1,993	$2,137.49
04/13/2013	USASMC	AR835-N14	$258.05	$276.11
05/22/2013	Process Instruments &	Model 2R130DA Triac 2R Series Pneumatic Actuator,Double Acting Rack & Pinion	$1,160	$1,252.80

	Controlls, LLC	Actuator with double travel stops,ISO / DIN mounting, Actuator size 130, Standard Buna seals (-5 F to 175 F) Model EPR-1000 Triac Positioner, Electro-Pneumatic, Rotary, 4-20mA, Flat Indicator ATD19T14 Insert		
5/30/2013	UC Davis Facilities	INSTALL 200 GALLON VERTICAL AIR RECEIVER TANK IN BAINER WIND TUNNEL FACILITY. FACILITY OPS SUPV MIC PRETTI VIEWED TANK AND INSTALLATION LOCATION. INSTALLATION REQUIRES LAG BOLTS INTO CONCRETE FLOOR. TANK IS CYLINDER SHAPED APPROX 6 FEET TALL AND 30 INCH DIAMENTER WITH FOUR LEGS. TANK DRAWING SUPPLY AIR FROM MAIN BAINER COMPRESSOR. REMOVABLE AIR SUPPLY HOSE. HOSE. PLUMBING REQUIRED-REGULATOR, CAP UNUSED PORTS, INSTALL DRAIN VALVE. REGULATOR/VALVES AND DIRECTIONS PROVIDED BY MAE AUBRYN COOPERMAN amcooperman@ucdavis.edu. VALVE AND REGULATOR ARE AVAILABLE TODAY. INSTALL TANK BETWEEN WIND TUNNELS. ORIENTATION DETERMINED BY REGULATOR OUTLET.	$1,412.41	$1,525.40
6/14/2013	Hose&fittings,etc	Hoses and general material for assembly of the setup	$298.61	$322.50
Total			$5,122.10	$5,514.30

9 Conclusion

From 22 March to 21 May I have been working at the Mechanical Engineering and Aerospace group of UC Davis on the microjet load control setup in the wind tunnel lab. During this time I was active in the ordering process, setup and first static tests that were done with the micro-jet system. The new aspects in the micro-jet system that were setup contained a 200 gallon air tank that was installed and permitted (which can be pressurized up to 80 PSI with current infrastructure), a 1 ½" NPT fitted regulator (SMCUSA NAR835-N14) that can operated manually (0-30 PSI), a 1 ½" NPT V-ported ball valve with 2 actuator/positioner systems, a highly accurate electric actuator/positioner (450 points of resolution) and a more responsive (90 degree closing/opening time within 2 seconds) electro pneumatic system that can be powered by the shop air that is present. However the electro pneumatic actuator/positioner cannot be used with the current National Instrument equipment because it is controlled using a 4-20mA signal. But for static testing the electric actuator/positioned is sufficient.

From the startup tests that where done, it was observed that for constant valve opening the $\Delta \mathbf{C_l}$ would be almost constant up to 8 degree angle of attack, for 12 degree angle of attack stall occurs resulting in a decrease in $\Delta \mathbf{C_l}$ like seen in Figure 28. Besides these results it was observed that the flow rate increased overtime even after the flow fully developed, however the influence measured was very small, below 5% of the mean measured flow rate or C_l.

When the angle sweep was studied the effect of the suction side (SS) jets and pressure side (PS) jets was compared to the reference angle sweep. This was done for 3 different flow rates. In the report these are referred to case 1(low flow rate, 20% stroke $C\mu_{SS}$ = 1.42E-04, $C\mu_{PS}$ =1.46E-04), case 2 (moderate flow rate, 40% stroke $C\mu_{SS}$ = 2.08E-03, $C\mu_{PS}$ = 2.06E-03), case 3 (high flow rate, 60% stroke $C\mu_{SS}$ = 5.59E-03, $C\mu_{PS}$ =5.00E-03) and case 4 which was equal to case 3 but had fewer data points. In some of the results case 3 and 4 were disregarded because the way the tests were conducted proved to form complications in the flow properties of the microjets. Maintaining steady flow conditions before and after the tank was refilled in 1 experiment proved to be a challenge. For the highest flow rate (115 SCFM) the jets can only be used for 20 seconds before the tank pressure drops below 15 PSI, but it takes more than 6 seconds to stroke the valve to 60% with the electric actuator.

The max C_l was in most cases found at the same angle of attack, there were 2 exceptions for the in bots SS and PS of case 1, here the SS jets resulted in a $C_l$max for 2 degrees below the reference no jet case and for the PS jets Clmax was found at a 2 degree higher angle of attack.

As was to be expected the influence of the microjets is not a purely vertical shift of the C_l-α curve. For case 1 and 2 the SS microjets resulted in a slight increase of $|\Delta C_l|$ for low angles of attack, for high angles $|\Delta C_l|$ increased more rapidly. For the PS microjets the a different pattern was found for case 1 and 2. It seems that for low flow rates the PS microjets disturb the laminar flow resulting in a decrease in lift rather than an increase.

It was observed that the slope of the Cl-α curve is lower when the microjets are used compared to the reference case. The slope dCl/dα proved to be about 20% lower for the SS microjets. The same result was found for case 1 with the PS microjets hooked up, but now the slope increased for increasing microjet flowrates, case 3 with PS microjets even has a higher slope compared to the reference.

The relationship between ΔCl and α was studied and could be described by a 2nd order polynomial as a function of the angle of attack α for both the SS and PS jets. For the SS microjets there was a reoccurring profile, this is however not the case for the PS microjets. For case 1 there was a linear relationship between α and ΔCl and for case 2 could best be described by a 2^{nd} order polynomial. Case 3 was inconsistent for both the SS and PS jets. The relationship between the Cμ and the angle of attack α proved to be linear in all SS and PS jet cases.

It is worrisome that the ΔCl-α curves of this research compared to earlier research done by A.M. Cooperman do not match. This could be due to the fact that the Reynolds number for which the tests were conducted are different. In this research all experiments were done at Re = 500,000, the data used from the research of A.M. Cooperman were done at Re = 1,000,000. In this research it was also noted that the tubing of the microjets cause interference to the balance, but it is unclear how much of a factor this is.

The costs that were made to install the tank and buy the equipment that was needed are steep at a $5514.30. This was caused by the fact that the Electric valve did not meet the requirements, the open and closing time at about 12 seconds is to slow to do close loop control, therefore a faster electro-pneumatic positioner in combination with a new actuator were bought. Also the installation of the Air tank proved to be more expansive than was thought beforehand.

10 Discussion and recommendations

For the results that were found for the higher flow rates (±115 SCFM, Cμ = 5.0E-03) it proved to be problematic to keep the jet flow conditions steady throughout the experiment. For the results to be consistent it is important that the microjet flow is fully developed and that the supply pressure remains constant throughout the experiment. From the 22.5 seconds startup experiment it is know that it takes about 8 to 10 seconds for the flow to fully develop, however after about 18 seconds the air tank is empty, meaning that with one tank of air only 1 or at most 2 measurements can be done. This means that the tank needs to be refilled about 3 times which would take more than an hour in which the testing conditions could have changed (temperature, air pressure). It would be advisable to fill the tank up to higher pressures to ensure more testing time. Another idea would be to refill the tank during testing, but for this to work an alternative to the shop air would be needed which would work at much higher flow rates.

The offset of +2 degrees angle of attack that was found afterwards for the suction side jet experiments was accounted for in the results section. What might have occurred was that overnight someone touched the setup and changed the angle of attack slightly, but it might be that some other equipment was also touched. Therefore to be sure the results are correct it would be best to redo one of the angle sweeps to check this. Besides this there was no new reference taken after the pressure side jets were setup. Because there is a negative ΔCl for jet flow rates of about 20 SCFM (Cμ = 1.4E-04) it is questionable if the reference is correct.

The interference to the balance caused by the microjet tubing results in an unknown error. It is difficult to say what the influence is for the different flow rates. It is advisable to look closer at this problem and to look for ways minimize the interference of the tubing on the balance.

For the open and closed loop testing the electric actuator will be too slow. The electro-pneumatic actuator and positioned will be able to fully open or fully close in 1.5 seconds, which is sufficient for open and close loop testing. However new hardware is needed to control the electro-pneumatic actuator and positioner because the current National Instrument system cannot output a 4-20 mA signal. There are several options to look at: the 2 main options are a NI Compact DAQ module or NI DAQ card that output a 4-20 mA signal, the alternative is to build a device that can produce a 4-20 mA signal from a 0-10V signal using an Operational Amplifier or something of this kind.

11 Bibliography

Anon., 2013. [Online]
[Accessed 30 5 2013].

Anon., n.d. *SMCUSA.* [Online]
Available at: http://www.smcusa.com/top-navigation/cad-models.aspx/15833
[Accessed 30 5 2013].

Barlow, J. B., Rae, W. J. H. & Pope, A., n.d. *Low Speed Wind Tunnel Testing.* s.l.:s.n.

Cooperman, A. M., 2012. *Windtunnel Testing of Microtabs and Microjets for Active Control of Wind Turbine Blades,* Davis: s.n.

Haslego, C., 2011. *cheresources.com.* [Online]
Available at: http://www.cheresources.com/content/articles/fluid-flow/valve-sizing-and-selection?pg=1
[Accessed May 2013].

LB, n.d. *Vertical Air Receiver 200 Gallon.* [Online]
Available at: http://www.mantank.com/pdf/Parts/302426/302426.pdf
[Accessed 30 5 2013].

M. Gaunaa, P. A., 2009. Load reduction using pressure differnce on airfoil for control of trailing edge flaps. *European Wind Energy Conference.*

TRIAC, n.d. *TRIAC Electro-Pneumatic Positioner.* [Online]
[Accessed April 2013].

TRIAG, 2012. *Pneumatic Rotary Actuators and Accessories.* [Online]
[Accessed 05 2013].

TRIAG, A.-T. C., n.d. *Electric Actuators,* Cincinetti: s.n.

TRIAG, A.-T. C., n.d. *INSTALLATION & MAINTENANCE MANUAL - TDC Servo Card for WED / XED Series Actuators,* s.l.: s.n.

Appendix A

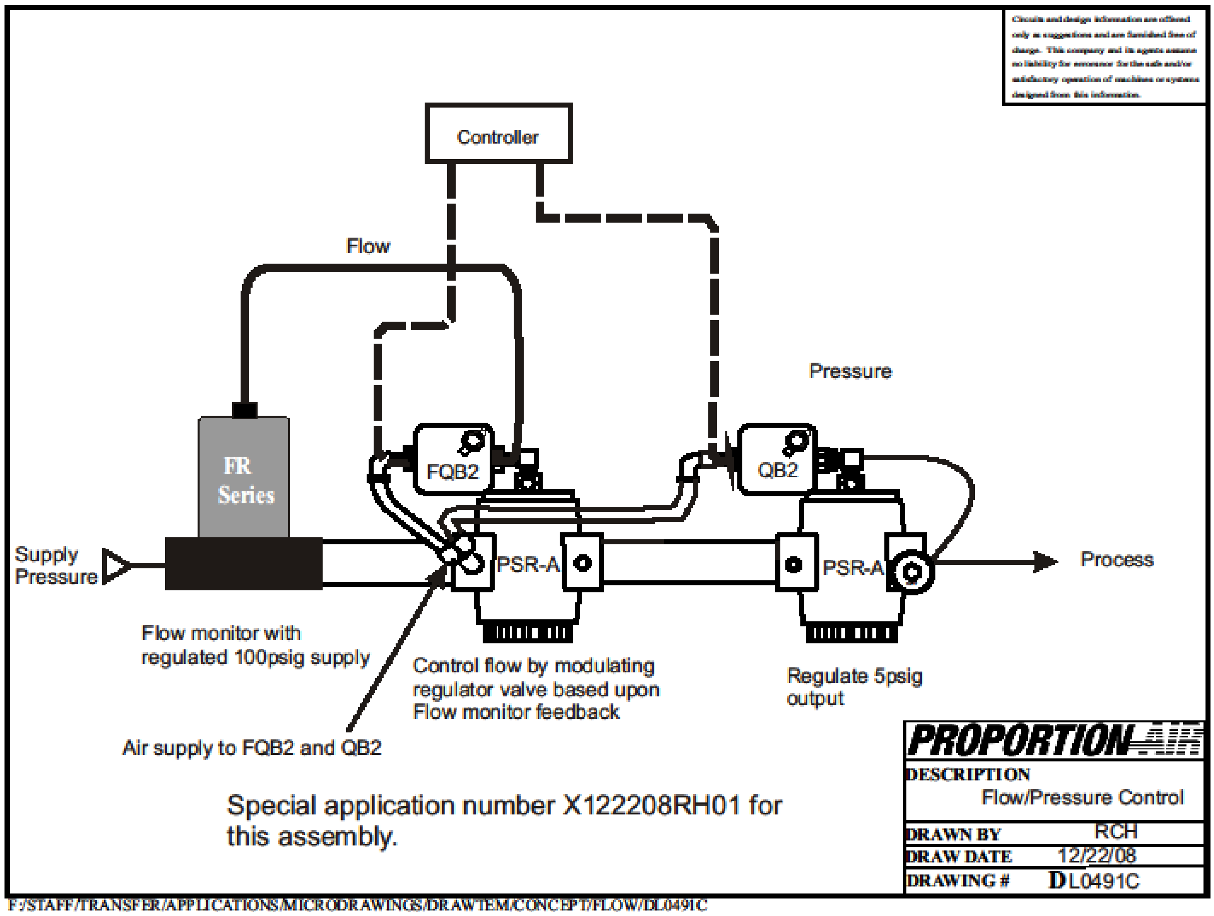

Figure 34 Proportion air product drawing

Appendix B

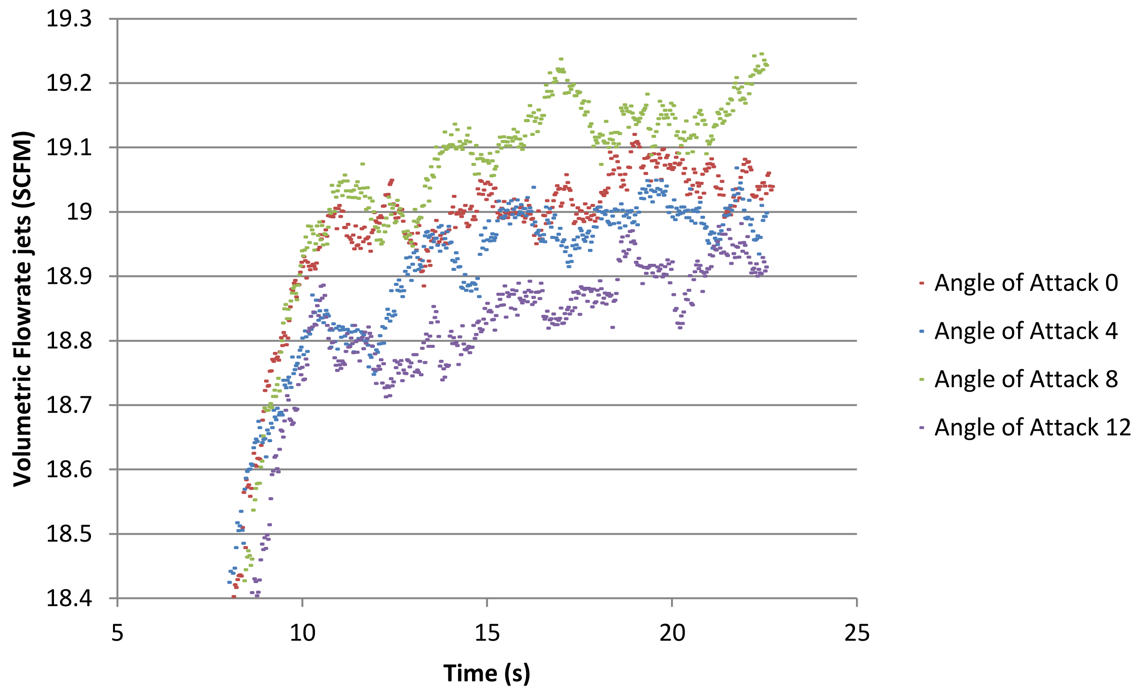

Figure 35 Volumetric flowrate (SCFM) course in time for 20% valve stroke.

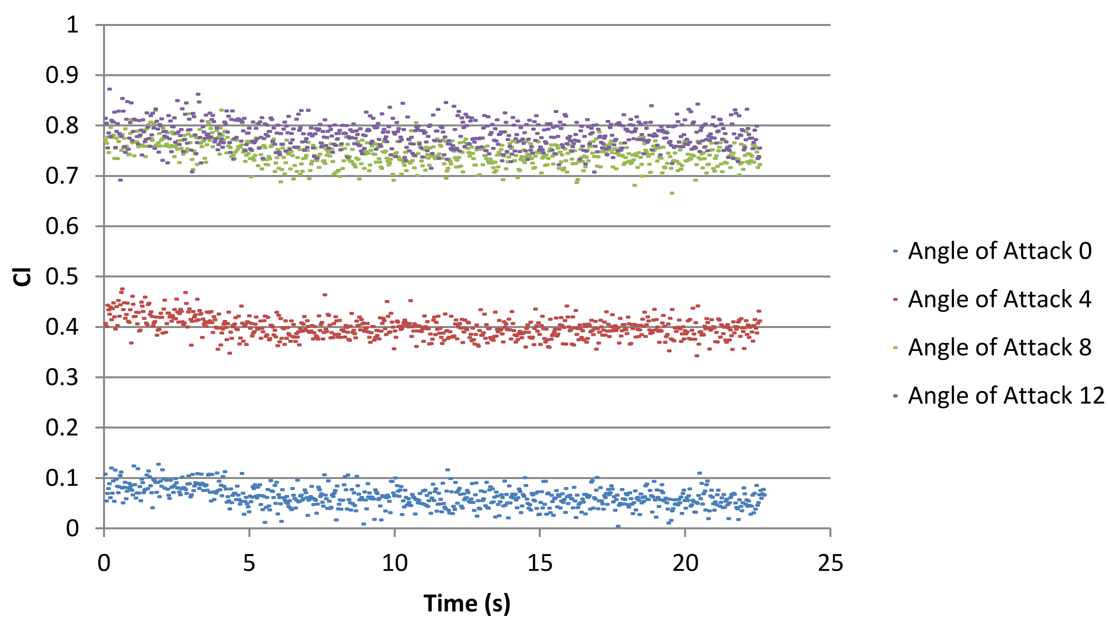

Figure 36 Cl course in time when jets are turned on up to 20% valve stroke.

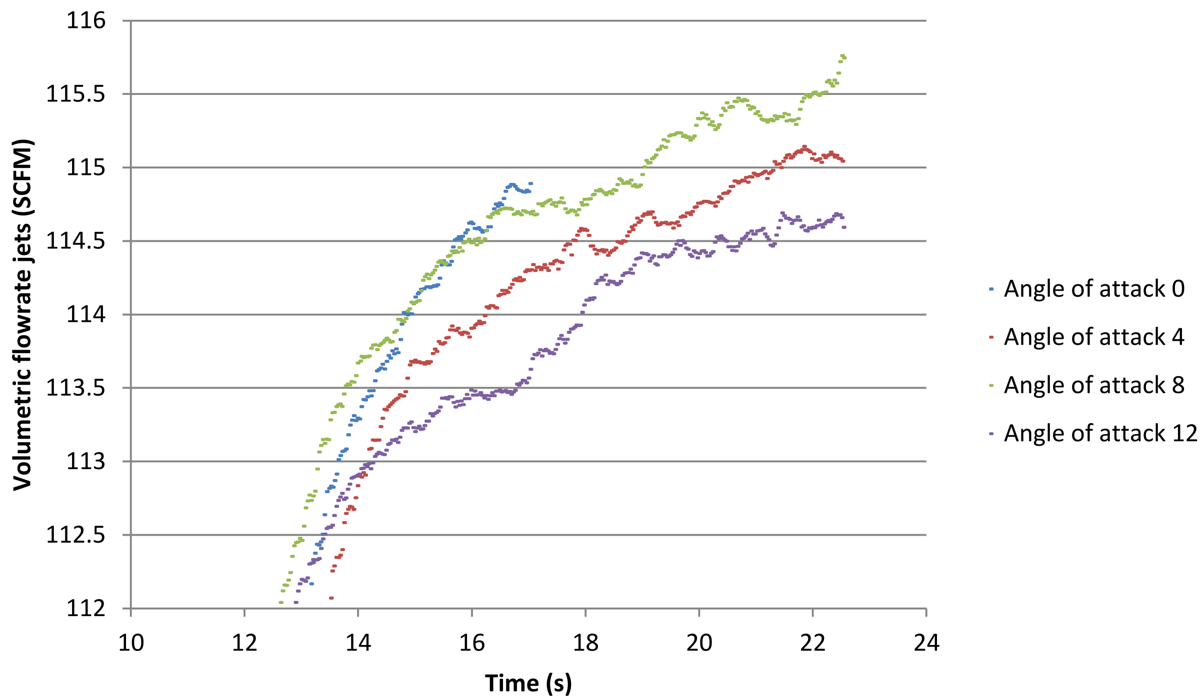

Figure 37 Volumetric flowrate (SCFM) course in time for 60% valve stroke.

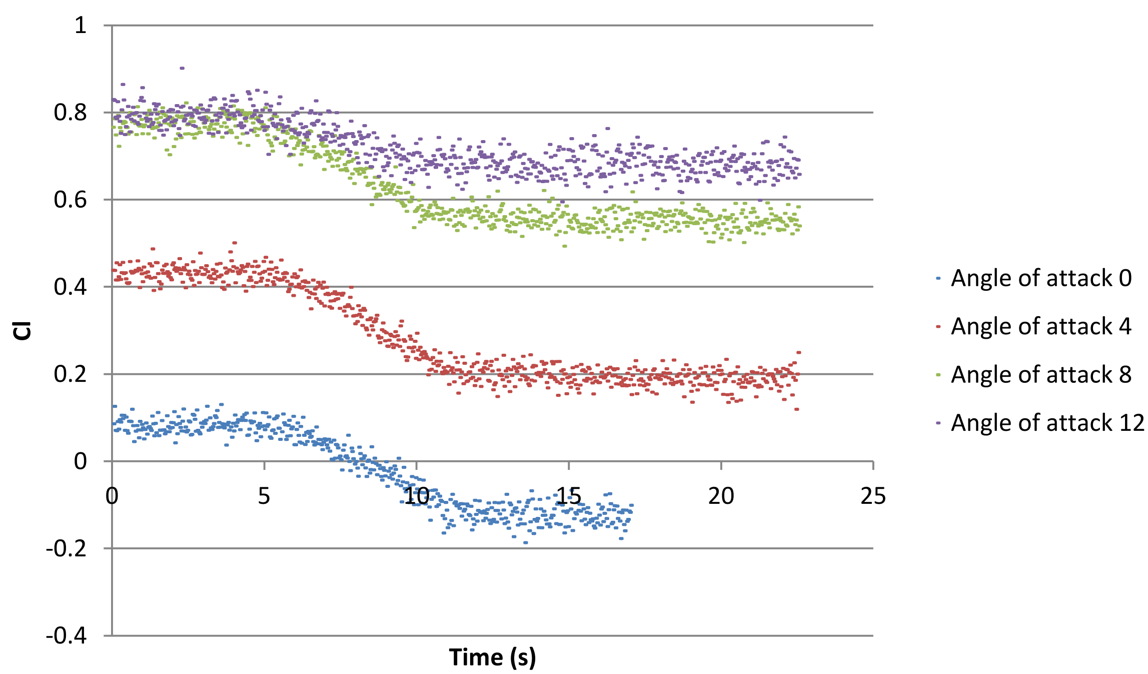

Figure 38 Cl course in time when jets are turned on up to 60% valve stroke.

Appendix C

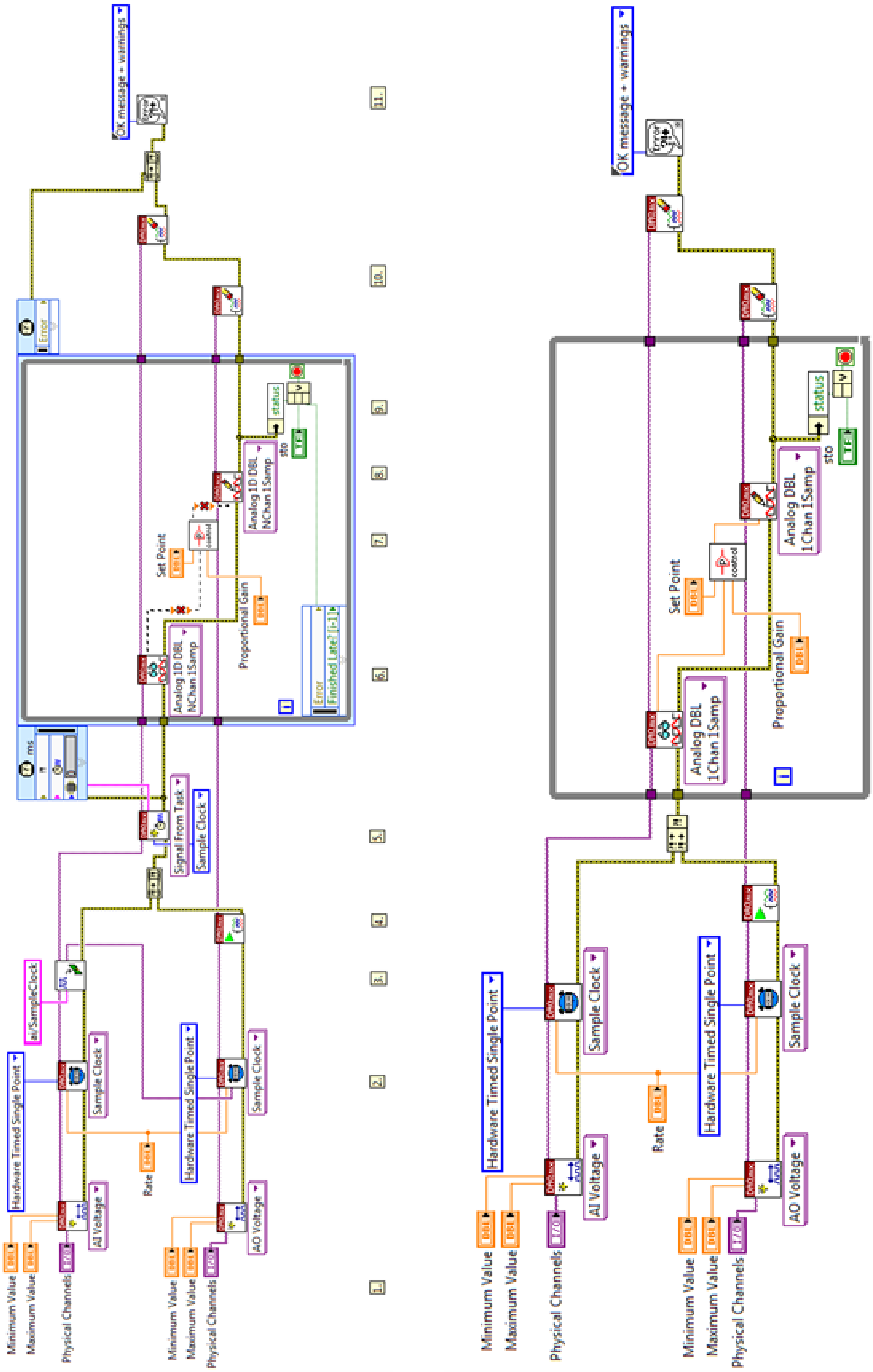

Figure 39 left unaltered proportional gain controller and right the altered proportional gain controller.

Appendix D

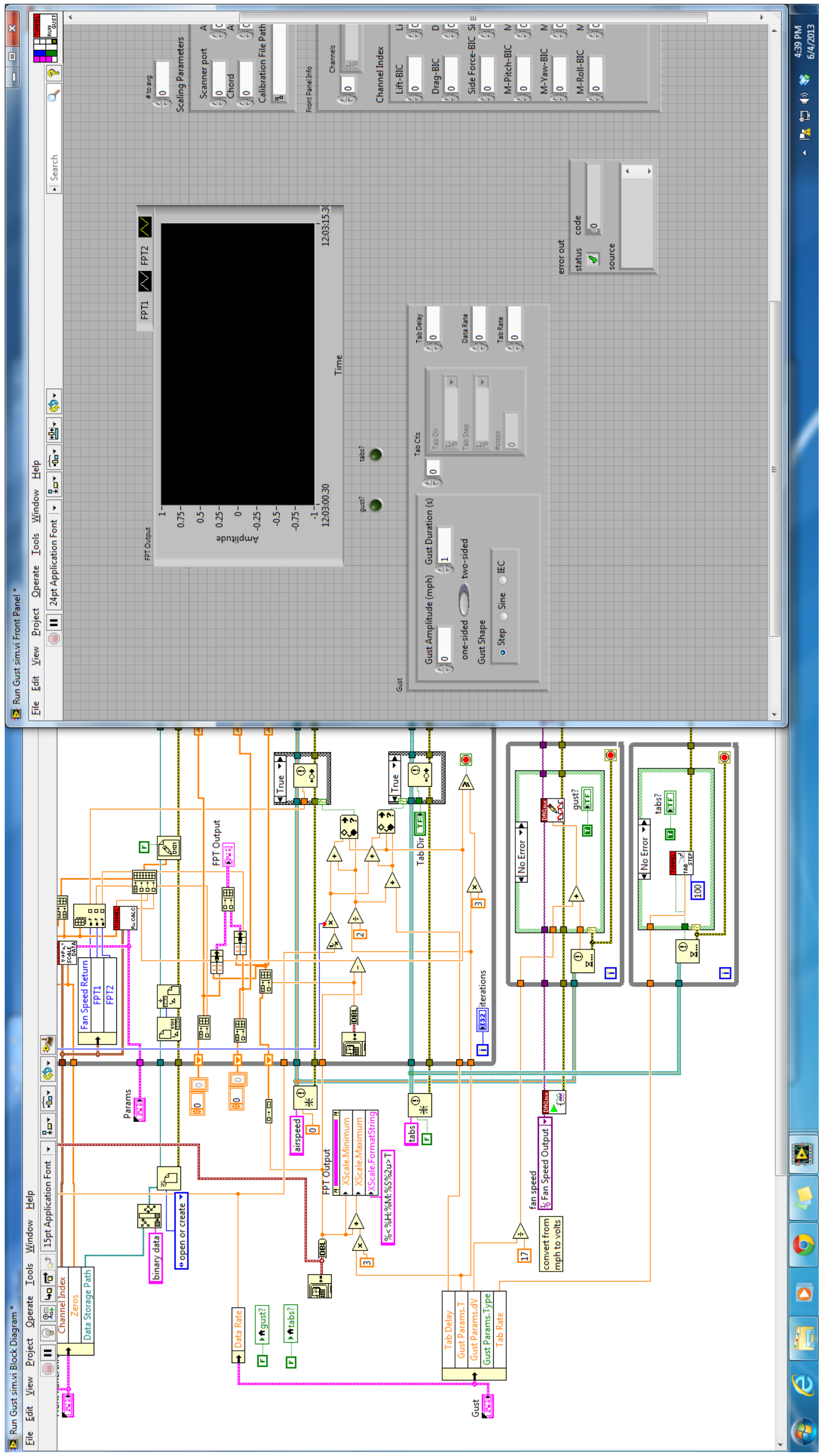

Figure 40 Block diagram and front panel of the altered Run Gust VI

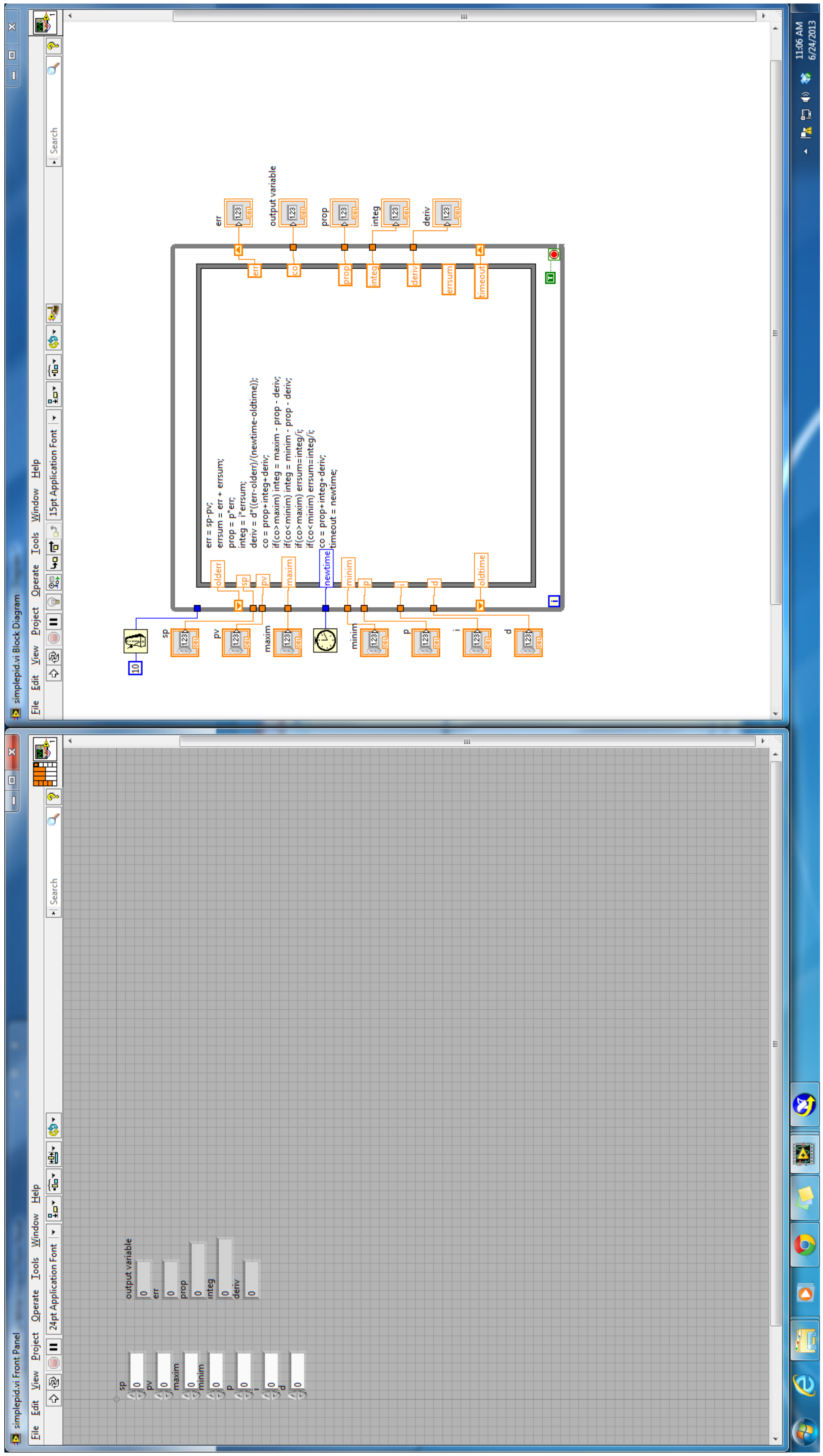

Figure 41 Block diagram and front panel of the PID controler